Article

Cell Reports

Microtubule Acetylation Is Required for Mechanosensation in *Drosophila*

Graphical Abstract

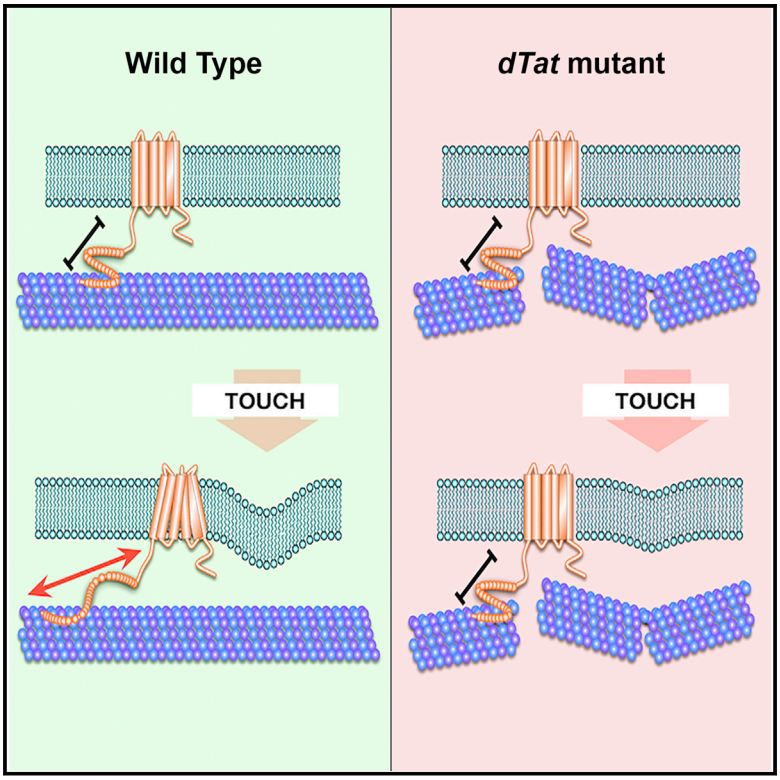

Authors

Connie Yan, Fei Wang, Yun Peng, ..., Yang Xiang, Stephen L. Rogers, Jay Z. Parrish

Correspondence

srogers@bio.unc.edu (S.L.R.), jzp2@uw.edu (J.Z.P.)

In Brief

Yan et al. identify the major microtubule acetylase in *Drosophila* and show that the enzyme and microtubule acetylation broadly control mechanosensation, but not other sensory modalities. Acetylation is required for mechanosensation by the TRP channel NOMPC, and possibly other channels, by virtue of its effects on microtubule mechanical stability and/or dynamics.

Highlights

- dTAT acts as the major α-tubulin acetylase in *Drosophila*
- Microtubule acetylation broadly and specifically regulates mechanosensation
- dTAT is required for mechanosensation by the TRP channel NOMPC
- Acetylation tunes microtubule stability to control mechanosensation

Yan et al., 2018, Cell Reports *25*, 1051–1065
October 23, 2018 © 2018 The Authors.
https://doi.org/10.1016/j.celrep.2018.09.075

CellPress

Cell Reports
Article

OPEN ACCESS
CellPress

Microtubule Acetylation Is Required for Mechanosensation in *Drosophila*

Connie Yan,[1] Fei Wang,[2] Yun Peng,[1] Claire R. Williams,[1] Brian Jenkins,[3] Jill Wildonger,[3] Hyeon-Jin Kim,[4] Jonathan B. Perr,[4] Joshua C. Vaughan,[4,5] Megan E. Kern,[6] Michael R. Falvo,[6] E. Timothy O'Brien III,[6] Richard Superfine,[7] John C. Tuthill,[5] Yang Xiang,[2] Stephen L. Rogers,[8,9,*] and Jay Z. Parrish[1,10,*]

[1]Department of Biology, University of Washington, Seattle, WA 98195, USA
[2]Department of Neurobiology, University of Massachusetts Medical School, Worcester, MA 01605, USA
[3]Department of Biochemistry, University of Wisconsin-Madison, Madison, WI 53706, USA
[4]Department of Chemistry, University of Washington, Seattle, WA 98195, USA
[5]Department of Physiology and Biophysics, University of Washington, Seattle, WA 98195, USA
[6]Department of Physics & Astronomy, The University of North Carolina at Chapel Hill, Chapel Hill, NC 27599-3280, USA
[7]Department of Applied and Physical Sciences, The University of North Carolina at Chapel Hill, Chapel Hill, NC 27599-3280, USA
[8]Department of Biology, Integrative Program for Biological and Genome Sciences, The University of North Carolina at Chapel Hill, Chapel Hill, NC 27599-3280, USA
[9]Lineberger Comprehensive Cancer Center, The University of North Carolina at Chapel Hill, Chapel Hill, NC 27599-3280, USA
[10]Lead Contact
*Correspondence: srogers@bio.unc.edu (S.L.R.), jzp2@uw.edu (J.Z.P.)
https://doi.org/10.1016/j.celrep.2018.09.075

SUMMARY

At the cellular level, α-tubulin acetylation alters the structure of microtubules to render them mechanically resistant to compressive forces. How this biochemical property of microtubule acetylation relates to mechanosensation remains unknown, although prior studies have shown that microtubule acetylation influences touch perception. Here, we identify the major *Drosophila* α-tubulin acetylase (dTAT) and show that it plays key roles in several forms of mechanosensation. dTAT is highly expressed in the larval peripheral nervous system (PNS), but it is largely dispensable for neuronal morphogenesis. Mutation of the acetylase gene or the K40 acetylation site in α-tubulin impairs mechanical sensitivity in sensory neurons and behavioral responses to gentle touch, harsh touch, gravity, and vibration stimuli, but not noxious thermal stimulus. Finally, we show that dTAT is required for mechanically induced activation of NOMPC, a microtubule-associated transient receptor potential channel, and functions to maintain integrity of the microtubule cytoskeleton in response to mechanical stimulation.

INTRODUCTION

Mechanosensation is a signal transduction process in which mechanical forces are converted into the neuronal signals that mediate hearing, balance, proprioception, and touch. In the peripheral nervous system (PNS), this conversion is mediated by ion channels that are gated by mechanical stimuli (Coste et al., 2010; O'Hagan et al., 2005; Walker et al., 2000). Mechanosensitive ion channels appear to have evolved multiple times and, as a result, several different channel families contribute to mechanosensation in animals, notably including transient receptor potential (TRP) channels, epithelial Na^+ channel (ENaC)/degenerin family channels, and piezos (Katta et al., 2015). Mechanical force is thought to activate the channels by inducing conformational changes, and two distinct models have been proposed to explain how force gates these channels. In the force from lipids model, plasma membrane deformation generates the tension required for channel gating via direct interaction between the mechanoreceptor and lipids of the plasma membrane (Christensen and Corey, 2007; Kung, 2005). In the force from filaments model, the channel is tethered to a non-compliant structure by a gating spring, and movement of the membrane-bound channel relative to the immobile structure induces tension within the spring to open the channel (Howard and Hudspeth, 1987; Jin et al., 2017; Liang et al., 2013). In this model, the gating spring is an elastic tether that connects the channel to extracellular structures, such as the extracellular matrix, or intracellular components, such as the cytoskeleton (Jin et al., 2017).

Our understanding about how tethered mechanoreceptors interact with the cytoskeleton largely comes from recent studies of mechanosensitive TRP channels. Notably, mammalian TRPV1 and *Drosophila* TRPN/no mechanoreceptor potential C (NOMPC) directly interact with microtubules (Cheng et al., 2010; Prager-Khoutorsky et al., 2014). In mammalian osmosensory neurons, TRPV1 binds a dense network of subcortical microtubules via cytoplasmic tubulin-binding motifs (Prager-Khoutorsky et al., 2014). Under hypertonic conditions, cells shrink and their membranes press against microtubules to generate an elastic compression that opens the channel. NOMPC possesses an elongated N-terminal cytoplasmic domain with 29 tandem ankyrin repeat (AR) domains that bind to microtubules (Cheng et al., 2010; Zhang et al., 2015). NOMPC forms tetramers in which the AR domains are organized into a quadruple bundle of helical, spring-like structures (Jin et al., 2017). The AR domains and microtubule interactions are necessary for NOMPC

This is an open access article under the CC BY-NC-ND license (http://creativecommons.org/licenses/by-nc-nd/4.0/).

touch-evoked responses, leading to the model that the AR helical elements function as a gating spring (Howard and Bechstedt, 2004; Jin et al., 2017; Liang et al., 2013; Zhang et al., 2015). Since direct interaction with the microtubule cytoskeleton is necessary for TRPV1 and NOMPC to function as mechanoreceptors, modulating mechanical properties of microtubules could be a control point for these channels.

Post-translational modifications of microtubules regulate their function during mechanosensation in several model systems. In *C. elegans*, the α-tubulin acetylase MEC-17 was identified in a screen for mutations with impaired touch sensitivity (Chalfie and Au, 1989). MEC-17 was the founding member of a family of α-tubulin acetylases with conserved homologs in all of the organisms that possess cilia (Akella et al., 2010). Depleting zebrafish MEC-17 produced a variety of developmental defects in embryos, including reduced startle responses to touch (Akella et al., 2010). In mice, mutants lacking the *Atat1* homolog in sensory neurons exhibited reduced mechanosensitivity and were unresponsive in assays for touch and pain (Kalebic et al., 2013b; Kim et al., 2013). These studies broadly implicate microtubules as conserved elements in mechanosensation and highlight a key regulatory role for acetylation.

Microtubule acetylation was discovered >30 years ago (L'Hernault and Rosenbaum, 1985), yet understanding of its biological function was hindered until the recent identification of α-tubulin acetylases. α-Tubulin acetylation occurs on lysine 40 (K40) in the microtubule lumen and has generally been associated with populations of long-lived microtubules. Recent studies in which individual microtubules were mechanically stressed by repeated cycles of bending showed that they could be damaged, resulting in decreased microtubule stiffness and localized material fatigue (Portran et al., 2017). K40 acetylation enhanced microtubule flexibility and increased mechanical resilience by altering the lattice structure, allowing microtubules to comply with deformative forces without breaking (Xu et al., 2017) and suggesting that α-tubulin acetylation regulates the mechanical resilience of microtubules. If the primary role for K40 acetylation is to tune microtubule mechanical properties, how might this biochemical activity relate to its requirement during mechanosensation?

Here, we report the identification of *Drosophila* α-tubulin acetylase (dTAT) and our characterization of its role in mechanosensation. dTAT is broadly required for α-tubulin acetylation and is enriched in the PNS. Blocking α-tubulin acetylation broadly affected mechanosensation, but not several other sensory modalities, while causing minimal effects on dendrite morphogenesis in the PNS. Using calcium imaging, we found that mutation of *dTat* or non-acetylatable alleles of α-*Tubulin84B* (*αTub84B)* attenuated gentle touch responses of NOMPC-expressing class III dendrite arborization (c3da) neurons. We further found that dTAT is required for NOMPC-dependent mechanically induced membrane depolarization. However, dTAT does not regulate gentle touch responses via effects on NOMPC-microtubule interactions or NOMPC localization. Instead, we found that dTAT modulates mechanical stability and/or dynamics of microtubules to control gentle touch responses and other forms of mechanosensation. First, hyperacetylation or taxol-induced microtubule stabilization sensitize larvae to gentle touch. Second, taxol treatment rescues mechanosensory behavior defects of *dTat* and non-acetylatable *αTub84B* mutants. Third, *dTat* mutant sensory dendrites contain more microtubule plus ends during development and in response to mechanical stimulation than controls, reflecting an increase in mechanically induced microtubule breakage or dynamics. Thus, modulation of microtubule stability appears to be a critical control point for mechanosensation. We also observed that, as in mice, cells lacking dTAT exhibit greater cortical stiffness, although we do not know whether this activity contributes to mechanosensation.

RESULTS

dTAT Is the Major Microtubule Acetylase in *Drosophila*

Five different acetylases are capable of modifying α-tubulin in mammalian cells or *Caenorhabditis elegans*, including GCN5, elongator protein 3 (ELP3), N-acetylase 10 (NAT10), the ARD1-NAT1 complex, and α-tubulin acetylase (αTAT)/MEC-17 (Akella et al., 2010; Conacci-Sorrell et al., 2010; Creppe et al., 2009; Ohkawa et al., 2008; Shida et al., 2010). We tested *Drosophila* homologs of these acetylases (see STAR Methods for details on candidate identification) for roles in microtubule acetylation by depleting each candidate in S2 cells with RNAi and monitoring acetylated α-tubulin (acTb) levels by immunoblot (Figure 1A). Depletion of only one candidate, *CG3967*, resulted in loss of acTb. We conclude that CG3967 is the major αTAT in S2 cells and hereafter refer to it as dTAT.

Using the same strategy, we identified the α-tubulin deacetylase. In mammalian cells, both HDAC6 and Sirt2 deacetylate microtubules (Hubbert et al., 2002; North et al., 2003). We targeted *Drosophila HDAC6* and the two *Drosophila Sirt2*-related genes (*Sirt1* and *Sirt2)* with RNAi and found that acTb levels were only elevated by *HDAC6* double-stranded RNA (dsRNA) (Figure S1A). We corroborated these results by immunoblotting samples from $HDAC6^{KO}$, $Sirt1^{KO}$, and $Sirt2^{KO}$ null mutants (Figure S1B). Taken together, our data indicate that *Drosophila* α-tubulin acetylation is regulated by the antagonistic activities of dTAT and HDAC6.

The *dTat* locus is predicted to generate a long (L) and a short (S) isoform encoding 461 residue (50 kDa) and 291 residue (30 kDa) proteins, respectively (Figure 1B). Both isoforms share an N-terminal 201 residue catalytic domain but diverge in their C-terminal tails, which lack predicted secondary structure. To define the roles of the two isoforms, we synthesized GFP-tagged versions of each isoform using alternate codons ($dTat^{alt}$-*L* and -*S*) to make them resistant to RNAi. Both isoforms rescued microtubule acetylation in cells treated with dsRNA to deplete endogenous dTAT (Figure 1C). In contrast, catalytically inactive mutant versions of both isoforms (G133W, G135W; Topalidou et al., 2012) failed to rescue microtubule acetylation.

Prior studies have shown that αTAT interacts with microtubules *in vitro* (Akella et al., 2010; Kalebic et al., 2013a; Shida et al., 2010; Szyk et al., 2014). Likewise, GFP-tagged $dTAT^{alt}$-L and $dTAT^{alt}$-S exhibited robust co-localization with microtubules (Figures 1D and 1E). In contrast, catalytically inactive $dTAT^{alt}$-L^{GG} and $dTAT^{alt}$-S^{GG} mostly localized in the cytoplasm, suggesting that acetylase activity is required for microtubule localization.

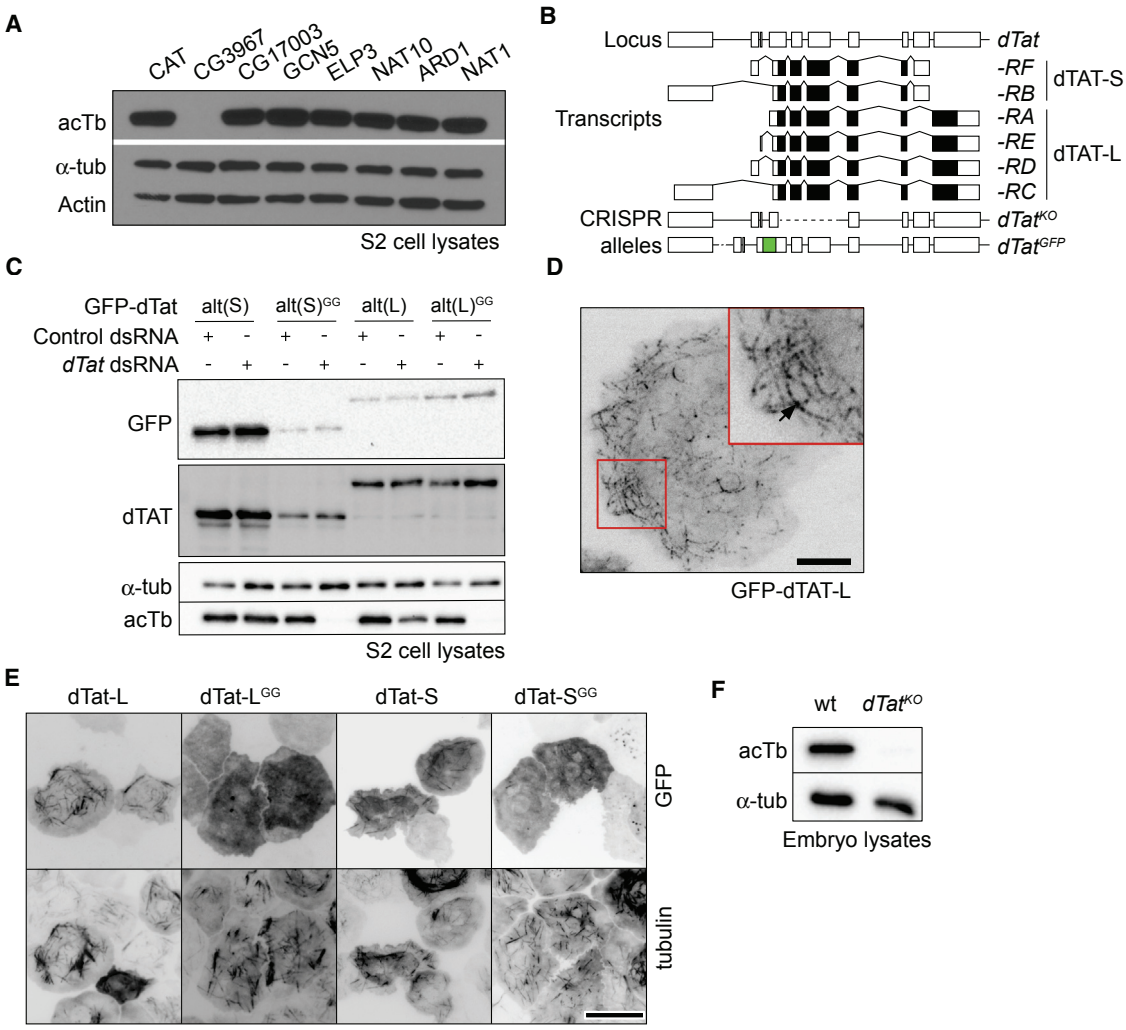

Figure 1. dTAT Is the Major Microtubule Acetylase in *Drosophila*

(A) Western blots of lysates from S2 cells treated with dsRNA to the indicated genes (CAT [chloramphenicol acetyltransferase]; used as a negative control).

(B) Schematic of the *dTat* locus which encodes six documented transcripts and two polypeptides (dTAT-L and dTAT-S) with alternative 3′ coding exons. Lines depict introns, and boxes depict coding (shaded) and non-coding (empty) exons. The $dTat^{KO}$ allele deletes the first three coding exons shared by all *dTat* transcripts and $dTat^{GFP}$ contains GFP coding sequences fused in-frame upstream of the start codon shared by all isoforms.

(C) Western blots of lysates from S2 cells treated with *dTat* or *CAT* dsRNA and additionally expressing RNAi-resistant versions of GFP-dTAT.

(D and E) Fluorescence microscopy of S2 cells expressing GFP-dTAT fusions showing the punctate, filamentous localization of GFP-dTAT-L (D) and co-localization of GFP-dTAT with α-tubulin (E). Scale bar, 5 μm in (D), 15 μm in (E).

(F) Western blotting of wild-type and $dTat^{KO}$ mutant embryo lysates.

See also Figure S1.

To study *dTat* function in flies, we deleted the first four exons of the gene to produce a null mutant ($dTat^{KO}$) (Figure 1B). Immunoblotting confirmed that $dTat^{KO}$ homozygous mutants lacked detectable acTb (Figure 1F). We conclude that dTAT is the major αTAT in flies, as in S2 cells.

dTAT Is Highly Expressed in PNS Neurons

To define biological functions of dTAT, we first examined *dTat* expression patterns. We fluorescence-activated cell sorting (FACS) isolated different GFP-labeled cell types and subjected the cell lysates to RNA-sequencing (RNA-seq) analysis (Figure 2A). Among the larval cell types that we surveyed, including muscle, epithelia, glia, and neurons, *dTat* expression is the highest in neurons. PNS neurons, particularly da neurons that mediate responses to mechanical, thermal, light, and proprioceptive stimuli, highly express isoforms for both dTAT-S and dTAT-L, suggesting that the PNS is likely an important functional site for dTAT.

Next, we examined dTAT protein distribution *in situ*. Consistent with our RNA-seq results, anti-dTAT immunoreactivity was concentrated in neurons, particularly PNS-da neurons (Figures 2B and 2C). dTAT exhibited elevated accumulation in the

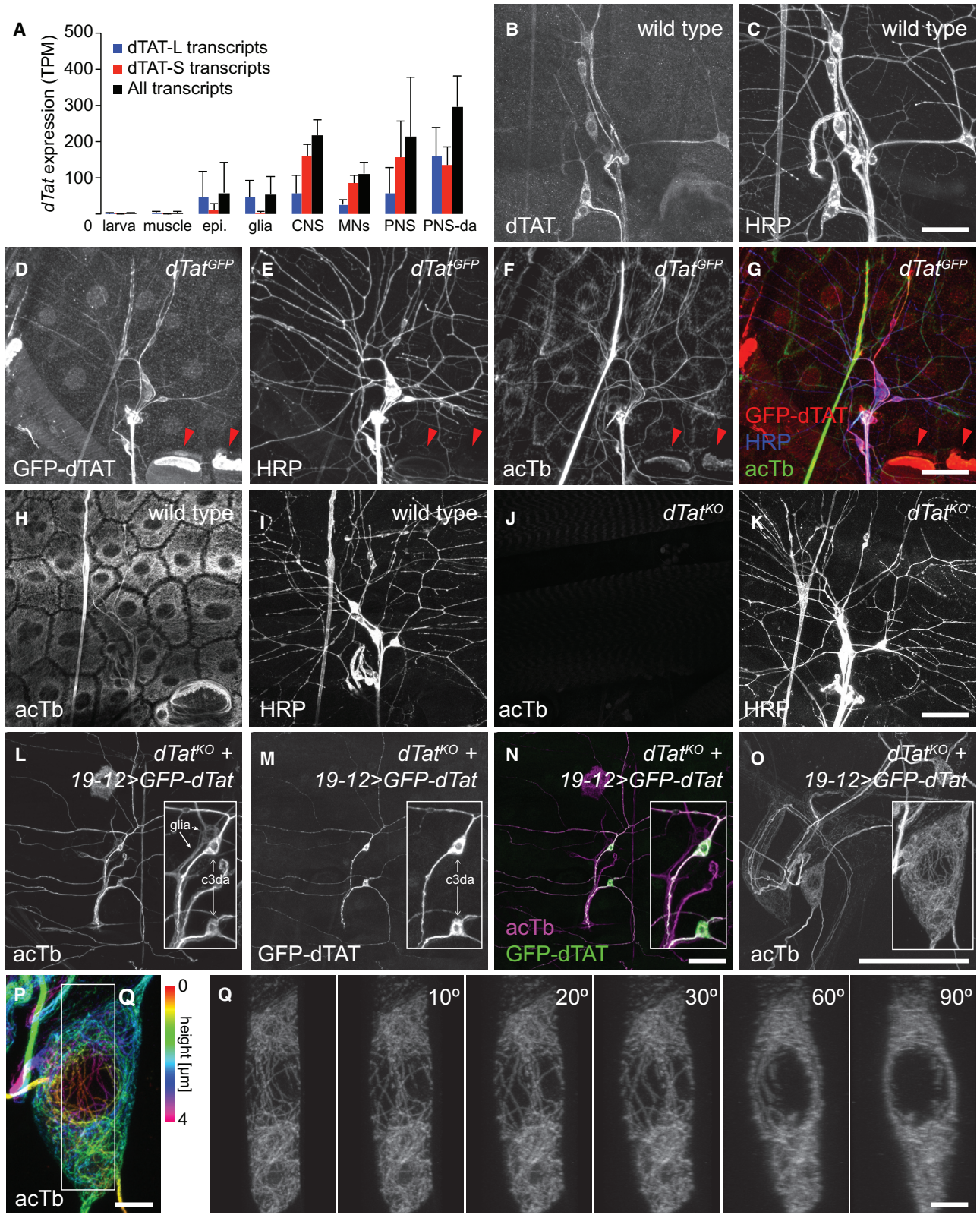

(legend on next page)

soma, axon, and primary dendrites, and undetectable levels in terminal dendrites of da neurons. Likewise, when we monitored GFP-dTAT distribution in larvae homozygous for an allele ($dTat^{GFP}$) that produces a GFP-dTAT fusion protein expressed from the endogenous *dTat* locus and supports microtubule acetylation *in vivo*, we found that GFP-dTAT was expressed most highly in PNS neurons (Figures 2D–2G), where it was enriched in the soma, axons, and primary dendrites but largely absent from terminal dendrites.

We next investigated patterns of acTb accumulation in wild-type and $dTat^{KO}$ mutant larvae. Immunostaining with a monoclonal antibody to acTb revealed a dense network of acTb immunoreactivity in all of the cells of the larval body wall, including prominent labeling of the PNS (Figures 2H and 2I). In contrast, $dTat^{KO}$ mutant larvae lacked detectable acTb immunoreactivity, demonstrating that *dTat* is required for tubulin acetylation (Figures 2J and 2K). Resupplying *dTat* selectively to mechanosensory c3da neurons via Gal4-mediated expression of the *dTat* long isoform containing an N-terminal GFP tag (*UAS-GFP-dTat-L*) rescued microtubule acetylation in a cell-autonomous manner, demonstrating that *dTat* expression in the PNS is sufficient for tubulin acetylation (Figures 2L–2N). This rescue assay allowed us to monitor acTb distribution in PNS neurons because acTb is present only in *dTat*-expressing cells. Similar to GFP-dTAT-L, acTb was enriched in the c3da soma, axons, and primary dendrites but largely absent from terminal dendrites. Thus, *dTat* is both necessary and sufficient for microtubule acetylation, and acTb distribution mirrors dTAT distribution in neurons.

In cultured mechanosensory dorsal root ganglion (DRG) neurons, acTb appears to be concentrated in a submembrane band (Morley et al., 2016). We therefore hypothesized that acTb would be similarly concentrated in mechanosensory c3da neurons. This is not what we found. Using expansion microscopy, which yields a spatial resolution of ~70 nm (Jiang et al., 2018), we observed a dense network of acTb throughout the soma that extended into axons and dendrites (Figure 2O). Although acTb immunoreactivity was restricted to a thin band around the nucleus of c3da neurons, the network of acTb coursed throughout other regions of the soma (Figures 2P and 2Q).

dTAT Is Required for Larval Mechanosensitivity

The microtubule cytoskeleton is involved in mechanosensation, particularly touch responses (Bounoutas et al., 2009; Tanner et al., 1998; Zhang et al., 2015), and mutations in mouse $\alpha TAT1$ and *C. elegans mec-17* and *atat-2* reduce mechanosensitivity (Morley et al., 2016; Shida et al., 2010; Topalidou et al., 2012). In *Drosophila*, gentle touch activates the TRP channel NOMPC, which relies on microtubule interactions for gating (Zhang et al., 2015), in c3da neurons to elicit stereotyped behaviors, including backward locomotion and turning (Kernan et al., 1994). We therefore tested *dTat* mutants for touch sensitivity defects. *dTat* mutation led to a ~67% decrease in gentle touch responses, with both $dTat^{KO}$ homozygotes and $dTat^{KO}$ in combination with a deficiency spanning the *dTat* locus ($dTat^{KO}/Df$) exhibiting similar defects (Figure 3A), suggesting that loss of *dTat* was the root cause of the defects. Next, we assayed gentle touch responses of mutants in which lysine 40 (K40) of the major α-*tubulin* isotype $\alpha Tub84B$, which accounts for >90% of α-tubulin expression in da neurons (Figure S2), is mutated to a non-acetylatable residue (Jenkins et al., 2017). We found that $\alpha Tub84B^{K40A}$ and $\alpha Tub84B^{K40R}$ mutants exhibited defects in gentle touch responses that were comparable to $dTat^{KO}$ mutants, strongly suggesting that microtubule acetylation regulates gentle touch responses (Figure 3A). Finally, $dTat^{KO}$, $\alpha Tub84B^{K40R}$ double mutant larvae exhibited comparable gentle touch defects to either single mutant alone, suggesting that *dTat* and $\alpha Tub84B$ function in the same pathway for gentle touch responses.

To determine the site of action for *dTat* in control of gentle touch responses, we next performed genetic rescue assays. Expressing *UAS-GFP-dTat-L* in c3da neurons rescued *dTat* mutant gentle touch defects, demonstrating that *dTat* function in c3da neurons is sufficient to support gentle touch responses (Figure 3B). Overexpressing *UAS-GFP-dTat-L* in c3da neurons of wild-type but not $\alpha Tub84B^{K40A}$ mutant larvae significantly enhanced gentle touch responses, suggesting that increasing acTb levels potentiates mechanosensitivity in c3da neurons. Consistent with this notion, $HDAC6^{KO}$ mutant larvae also exhibited heightened gentle touch responses (Figure 3B).

We next asked whether *dTat* was involved in other forms of mechanosensation, including harsh touch, vibration response,

Figure 2. dTAT Is Enriched in the Peripheral Nervous System

(A) RNA-seq analysis of *dTat* expression. Bars depict mean expression levels of *dTat* transcripts in the indicated cell types. TPM, transcripts per million. Error bars, SDs. N = 4+ independent samples for each condition.

(B–G) Distribution of endogenous dTAT. Maximum intensity projections of larval body walls immunostained with antibodies to dTAT (B) and horseradish peroxidase (HRP) to label sensory neurons (C).

(D–G) Maximum intensity projections of $dTat^{GFP}$ larval body walls stained with antibodies to GFP (D), HRP (E), and acTb (F).

(G) Overlay of dTAT-GFP, acTb, and HRP signals. We note high levels of dTAT-GFP and acTb in apodemes (red arrowheads), which are consistent with a prior characterization of acTb distribution (Jenkins et al., 2017).

(H–K) *dTat* is required for acTb accumulation *in vivo*. Maximum intensity projections are shown for wild-type third-instar larvae (H and I) stained with antibodies to acTb (H) and HRP (I) and $dTat^{KO}$ mutant third-instar larvae (J and K) stained with antibodies to acTb (J) and HRP (K).

(L–O) acTb distribution in sensory neurons. Maximum intensity projections are shown for $dTat^{KO}$ mutant third-instar larvae expressing *UAS-GFP-dTat-L* via *19-12-Gal4* and stained with antibodies to acTb (L) and GFP (M).

(N) Overlay of images from (L) and (M). Insets, zoomed images of cell bodies; arrows mark the cell types (c3da neurons and peripheral glia) labeled by *19-12-Gal4*.

(O) Maximum intensity projection of expanded body wall tissue from $dTat^{KO}$ mutant third-instar larvae expressing *UAS-GFP-dTat-L* via *19-12-Gal4* stained with acTb antibodies.

(P) Maximum intensity projection of c3da neuron from (O), with color marking the height within the specimen.

(Q) 3D rendering of acTb staining in the boxed portion of c3da neuron from (P) viewed en face or rotated as indicated.

Scale bars, 50 μm in (B–N), 20 μm in pre-expansion dimensions (O), and 2 μm in pre-expansion dimensions (P and Q).

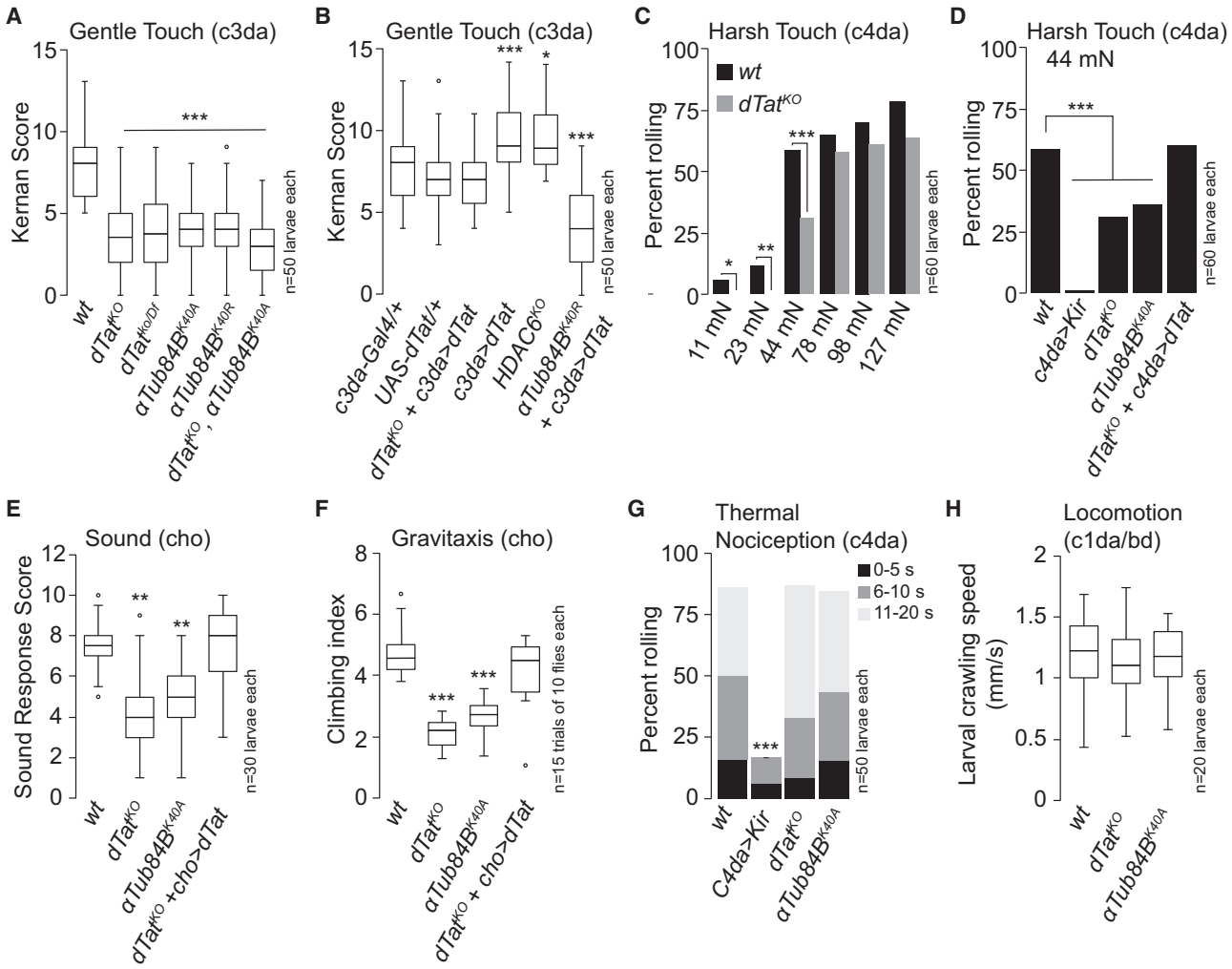

Figure 3. *dTat* Regulates *Drosophila* Mechanosensation

(A and B) *dTat* is necessary for gentle touch responses. Gentle touch responses are shown for *dTat* and non-acetylatable α*Tub84B* mutant larvae (A) and in *dTat* rescue and overexpression larvae (B). Boxplots depict larval behavioral responses of the indicated genotypes to gentle touch at 96 hr after egg laying (AEL). In this and subsequent panels, boxes mark first and third quartiles, bands mark medians, whiskers mark 1.5 × interquartile range (IQR), and outliers are shown as points. *p < 0.05, ***p < 0.001 compared to wild-type (WT); Kruskal-Wallis rank sum test with Dunn's post hoc test and Bonferroni correction for multiple comparisons.

(C and D) *dTat* is necessary for harsh touch responses.

(C) Bars depict the proportion of wild-type or *dTat* mutant larvae responding to von Frey fiber stimulation delivering the indicated amount of force. *dTat* mutants exhibit significant defects in response to 11, 22, and 44 mN stimulus. *p < 0.05, **p < 0.01, ***p < 0.001, compared to wild-type controls; unpaired t test with Welch's correction.

(D) Bars depict the proportion of larvae of the indicated genotype that exhibited nociceptive rolling in response to 44 mN von Frey fiber stimulation. ***p < 0.001 compared to wild-type; chi square test.

(E and F) Boxplots depict larval vibration responses (E) and adult gravitaxis (F) in the indicated genotypes. *p < 0.05, **p < 0.01, ***p < 0.001 compared to wild-type; Kruskal-Wallis rank sum test with Dunn's post hoc test and Bonferroni correction for multiple comparisons.

(G) Bars depict the proportion of larvae that exhibited nociceptive rolling responses to stimulus with a 39.5°C thermal probe. Responding larvae were grouped in three bins according to response latency: 0–5 s (black), 6–10 s (gray), and 11–20 s (light gray). ***p < 0.001 compared to wild-type; chi square test.

(H) Boxplots depict the rate of larval locomotion for the indicated genotypes. *dTat* and α*Tub84B* mutants exhibited comparable rates of locomotion to wild-type (Kruskal-Wallis rank sum test). The number of larvae or adults tested is shown for each condition.

See also Figure S2.

and gravitaxis. Harsh touch activates c4da nociceptive neurons to elicit stereotyped nocifensive rolling responses (Zhong et al., 2010), so we stimulated larvae with von Frey filaments and monitored touch-evoked rolling responses as a measure for *dTat* function in harsh touch. $dTat^{KO}$ mutant larvae exhibited significantly reduced nocifensive responses to stimuli ranging from 11 to 44 mN but not from 78 to 127 mN (Figure 3C), revealing that harsh stimuli can bypass the requirement for acTb in mechanosensory responses. These mechanonociceptive defects likely reflect a cell-autonomous role for acetylation in c4da neurons, as

dTat^{KO} mechanonociception defects were phenocopied by non-acetylatable α*Tub84B*^{K40A} mutants and rescued by c4da-specific *GFP-dTat-L* expression (Figure 3D).

Whereas da neurons mediate responses to gentle and harsh touch, chordotonal (cho) neurons mediate vibration and gravity responses (Kamikouchi et al., 2009; Zhang et al., 2013). To determine whether *dTat* was required for mechanosensory responses in cho neurons, we assayed *dTat* mutants for defects in larval vibration responses and adult gravitaxis. Wild-type larvae exhibited a stereotyped startle response to vibration delivered in the form of a sound stimulus (70 dB, 500 Hz tone) that was compromised in *dTat*^{KO} and non-acetylatable α*Tub84B*^{K40A} mutants (Figure 3E). As with touch responses, these defects likely reflect a neuronal requirement for *dTat* as expressing *UAS-GFP-dTat-L* in cho neurons of *dTat*^{KO} mutants rescued the vibration startle defects. Finally, adult gravitaxis behavior was impaired in *dTat*^{KO} and non-acetylatable α*Tub84B*^{K40A} mutants, and gravitaxis defects could be rescued by neuronal expression of *UAS-GFP-dTat-L* in *dTat*^{KO} mutants (Figure 3F). These results demonstrate that *dTat* and microtubule acetylation are broadly required for *Drosophila* mechanosensation.

These mechanosensory defects could reflect general defects in sensory transduction or a more specific effect on mechanosensation. To differentiate between these possibilities, we assayed for *dTat* functions in other sensory modalities. First, we found that larval responses to noxious heat, which are mediated by c4da neurons (the very same neurons that mediate harsh touch responses) (Hwang et al., 2007), were unaffected in *dTat*^{KO} and non-acetylatable α*Tub84B*^{K40A} mutants (Figure 3G). Second, application of the TRPA1 channel agonist allyl isothiocyanate (AITC), which directly activates c4da neurons to elicit nocifensive escape responses (Kaneko et al., 2017), generated comparable responses in wild-type and *dTat*^{KO} larvae (56.6% + 7.1% of control and 60.1% + 6.8% of *dTat*^{KO} larvae exhibit nociceptive rolling within 30 s of AITC application; n = 6 trials of 50 larvae each). Third, we found that wild-type controls, *dTat*^{KO}, and non-acetylatable α*Tub84B*^{K40A} mutants exhibited comparable rates of larval locomotion (Figure 3H). These results demonstrate that *dTat* and microtubule acetylation do not broadly regulate sensory transduction but instead preferentially affect mechanosensory responses.

dTAT Is Largely Dispensable for Dendrite Morphogenesis

How might dTAT influence mechanotransduction? Knock down of the ARD1-NAT acetylase, which reduces microtubule acetylation, and pharmacological inhibition of the microtubule deacetylase HDAC6, which increases acetylation, compromise dendrite growth in hippocampal cultures (Ageta-Ishihara et al., 2013; Ohkawa et al., 2008). Likewise, α-Tub84B K40 mutation affects dendrite branching in *Drosophila* c4da neurons (Jenkins et al., 2017). While each of these studies suggests a role for acetylation in dendrite development, both ARD1-NAT and HDAC6 target additional substrates, and α-tubulin K40 may have a structural role and may be subject to additional modifications, including methylation (Park et al., 2016). Thus, the roles of dTAT and α-tubulin acetylation in dendrite development are still unclear.

We therefore examined whether defects in mechanosensory neuron morphogenesis caused by *dTat* mutation may contribute to mechanosensory defects. Using *nompC-Gal4* (Petersen and Stowers, 2011) to visualize c3da neurons, which mediate larval responses to gentle touch, we found that *dTat* mutation had no obvious effect on dendrite arborization (Figures 4A–4D). Similarly, when we used antibody staining to label cho neurons, which mediate larval response to vibration, we found that *dTat* mutation had no obvious effect on cho neuron morphogenesis (Figures 4E–4G). Thus, *dTat* is dispensable for dendrite morphogenesis in mechanosensory c3da and cho neurons.

Next, we monitored the effects of *dTat* mutation on dendrite morphogenesis in c4da neurons using *ppk-CD4-tdGFP* (Han et al., 2011) to selectively visualize c4da dendrite arbors. *dTat* mutant c4da dendrites had no overt defects in the establishment or maintenance of dendrite coverage (Figures 4H and 4I), in overall growth (Figure 4J), or in growth dynamics (Figure 4L). However, we noted a minor but consistent effect on the number and position of dendrite branch points (Figures 4K and S3). Prior studies suggested that microtubule acetylation regulates microtubule susceptibility to katanin severing (Sudo and Baas, 2010), but we found that *dTat* mutation had no effect on *katanin*-induced dendrite arbor remodeling (Figure S3). These results demonstrate that although *dTat* plays a minor role in c4da neuron dendrite development, it is not broadly required for mechanosensory neuron morphogenesis. Similarly, mouse *Atat1* (Morley et al., 2016) and *C. elegans mec-17* (Akella et al., 2010; Shida et al., 2010) are largely dispensable for sensory neuron morphogenesis, suggesting that the wide-ranging effects of dTAT on mechanosensation are likely caused by other mechanisms.

dTat Is Required for NOMPC-Dependent Mechanotransduction

The *dTat* mutant mechanosensory defects could reflect defects in mechanosensation or in transmission downstream of mechanosensation. To differentiate between these possibilities, we used calcium imaging to measure mechanosensory responses of c3da neurons in wild-type and *dTat* mutant larvae. We immobilized semi-intact larval preparations expressing the transgenic calcium sensor GCaMP6s in c3da neurons, provided mechanical stimulus via focal body wall displacement, and monitored calcium responses in c3da neurons using a confocal microscope (Figure 5A). Consistent with previous reports (Yan et al., 2013), we found that touch stimulus induced robust calcium responses in c3da neurons (Figure 5B). In wild-type larvae, increased stimulus strength led to a progressive increase in calcium responses over a low range of stimuli (10–40 μm displacement), beyond which responses reached plateau (Figure 5C). *dTat*^{KO} and α*Tub84B*^{K40A} mutants exhibited significant reductions in touch-induced calcium transients that were most pronounced in the low force range. For example, 30 μm displacement yielded half-maximal calcium responses in wild-type larvae and negligible responses in *dTat*^{KO} and α*Tub84B*^{K40A} mutants. These defects were progressively attenuated with increased stimulus strength, suggesting that the mechanosensory requirement for *dTat* in c3da neurons can be overcome by increasing stimulus strength, similar to what we observed in c4da neurons (Figures 3C and 5C). These results further suggest

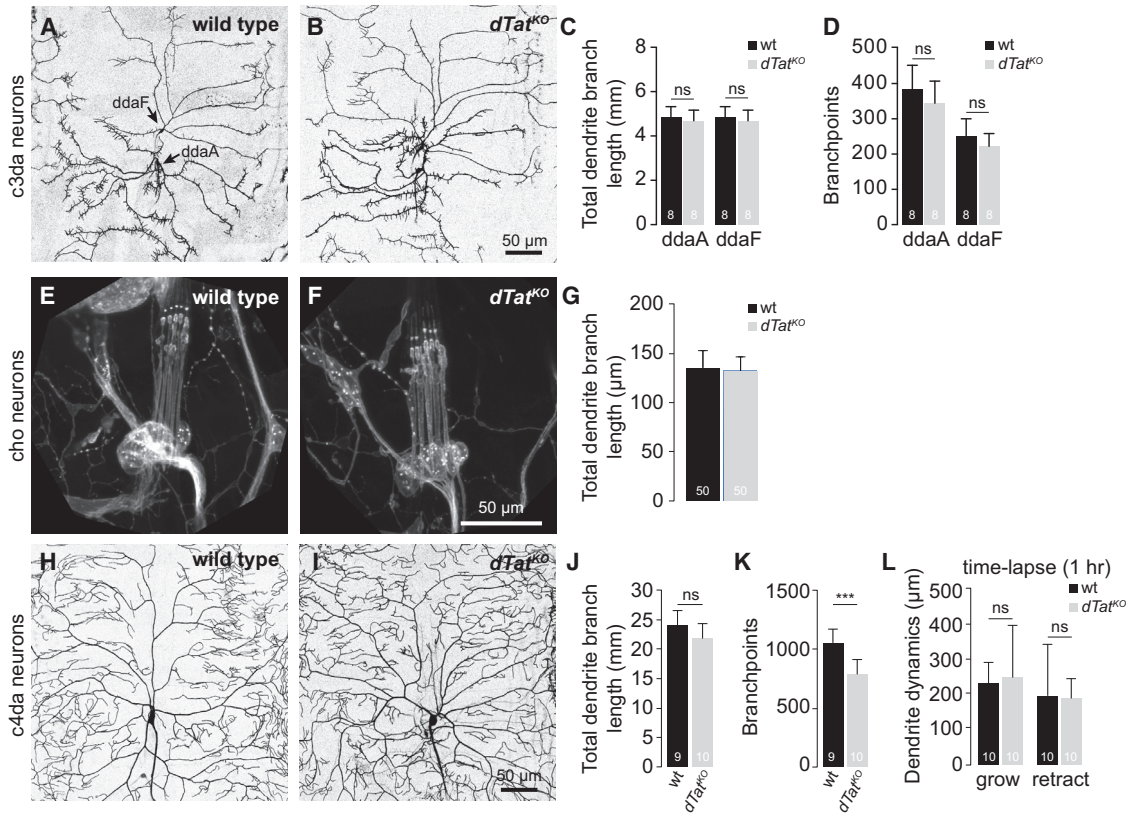

Figure 4. *dTat* Is Largely Dispensable for Dendrite Morphogenesis in Mechanosensory Neurons

(A and B) Representative images of (A) wild-type control and (B) $dTat^{KO}$ mutant c3da neurons labeled with *nompC-Gal4, UAS-mCD4-tdGFP*.

(C and D) Means and SDs are shown for (C) dendrite branch length and (D) number of branch points of the c3da neurons ddaA and ddaF.

(E and F) Representative images of cho neurons from (E) wild-type and (F) $dTat^{KO}$ mutant third-instar larvae labeled with anti-HRP antibodies.

(G) Bar graphs depict means and SDs for cho dendrite length of the indicated genotypes.

(H and I) Representative images of c4da neurons labeled with *ppk-CD8-GFP* are shown for (H) wild-type and (I) $dTat^{KO}$ mutant third instar larvae.

(J–L) Means and SDs are shown for (J) dendrite branch length, (K) number of branch points, and (L) dendrite dynamics measured over a 1-hr time lapse (96–97 hr AEL).

***p < 0.001; ns, not significant compared to wild-type; unpaired t test with Welch's correction. The number of neurons analyzed for each sample is indicated. Scale bars, 50 μm.

See also Figure S3.

that *dTat* functions in PNS neurons to regulate mechanosensory responses.

Given that larval gentle touch responses require the NOMPC channel, whose function depends on microtubule interactions, we next conducted genetic epistasis analysis to determine whether dTAT and NOMPC function in the same pathway. While mutation in either *dTat* or *nompC* impaired larval gentle touch responses, *nompC* mutation had more severe effects (Figure 5D). Expressing tetanus toxin in c3da neurons to block their synaptic output resulted in an even stronger defect than *nompC* mutation (Figure 5D), suggesting that *nompC*-independent pathways contribute to gentle touch responses (Tsubouchi et al., 2012). If *dTat* and *nompC* function in independent pathways, we reasoned that *nompC; dTat* double mutants should have more severe defects than either single mutant alone. Instead, gentle touch defects of the double mutant and *nompC* mutants were indistinguishable (Figure 5D), suggesting that *dTat* and *nompC* function in the same genetic pathway for gentle touch.

We next tested whether *dTat* was required for NOMPC-mediated mechanotransduction. For these experiments, we first tested whether NOMPC expression could confer mechanosensitivity to neurons that were normally unresponsive to mechanical stimuli. Whereas many PNS neurons, including c1da, c3da, c4da, and cho neurons, express mechanosensitive ion channels, we found that motor neurons (MNs) do not, although MNs do exhibit high levels of *dTat* expression (Table S1; Figure 2A). Consistent with these expression data, when we conducted *in vivo* whole-cell recordings from leg MNs in the adult ventral nerve cord (Figure 5E), we found that mechanical neuropil stimulation did not produce a consistent response (Figures 5F and 5G). By contrast, when we expressed *UAS-nompC-GFP* in leg MNs, mechanical neuropil stimulation reliably evoked depolarizing responses. This mechanically evoked depolarization was abrogated by *dTat* mutation. Thus, NOMPC expression is sufficient to confer mechanosensitivity to MNs, and *dTat* is required for NOMPC-dependent mechanotransduction.

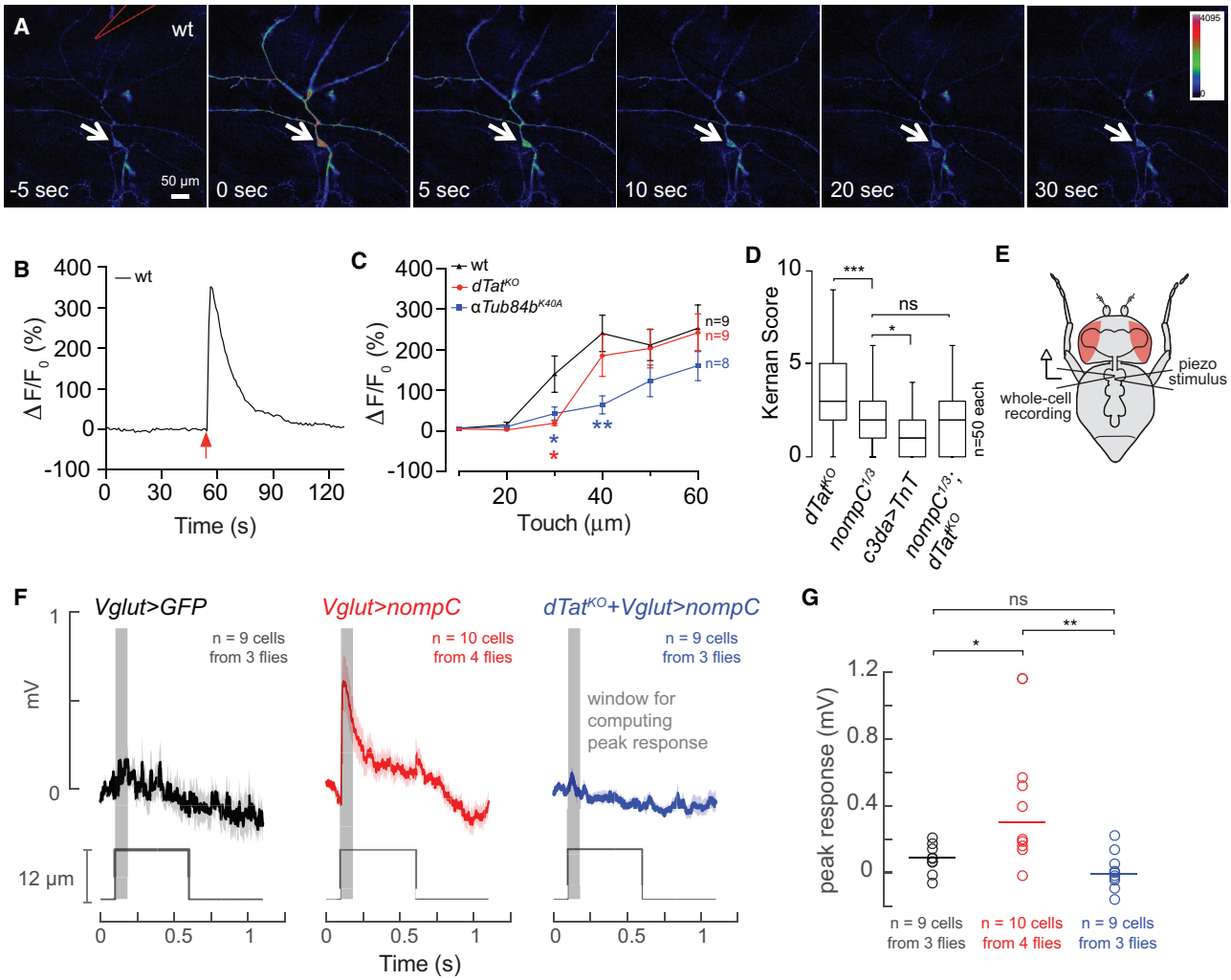

Figure 5. *dTat* Is Required for NOMPC-Mediated Mechanotransduction

(A) Calcium responses to mechanical stimulus delivered via a polished glass electrode (position marked in red in top left image) in larvae expressing *UAS-GCaMP6s* in c3da neurons (*nompC-Gal4*).

(B) Representative trace of calcium response measured from the c3da soma.

(C) Means and SDs for calcium responses [$\Delta F/F_0 = (F_{peak} - F_0)/F_0$] from larvae of the indicated genotypes in response to different mechanical stimuli. *$p < 0.05$, **$p < 0.01$ compared to wild-type; two-way ANOVA followed by Bonferroni's multiple comparisons test.

(D) Larval behavioral responses to gentle touch stimulus at 96 hr AEL are shown for the indicated genotypes. Bar graphs show means and SDs for Kernan scores. *$p < 0.05$, ***$p < 0.001$; ns, not significant compared to wild-type; Kruskal-Wallis rank sum test for multiple independent samples with Dunn's post hoc test and Bonferroni correction for multiple comparisons. Brackets indicate pairs being compared.

(E) Schematic for recording preparation used in (F and G).

(F) Average traces (±SEM) from whole-cell patch-clamp recordings for wild-type MNs expressing *UAS-GFP* (*Vglut > GFP*, left), wild-type MNs expressing *UAS-GFP-nompC* (*Vglut > nompC*, middle), and MNs from a $dTat^{KO}$ mutant larva expressing *UAS-GFP-nompC* ($dTat^{KO}$ + *Vglut > nompC*, right). Red lines depict mechanical stimulus.

(G) Scatterplot depicting mean (line) and individual measurements (points) of maximum depolarization minus baseline resting potential for the indicated genotypes. *$p < 0.05$, **$p < 0.01$; ns, not significant compared to wild-type; one-way ANOVA followed by Bonferroni's multiple comparisons test.

The number of independent samples measured for each genotype is shown in each panel.

See also Table S1.

We next tested hypotheses for how *dTat* regulates NOMPC function. First, microtubule acetylation plays established roles in intracellular transport (Bhuwania et al., 2014; Reed et al., 2006); thus, we tested roles for *dTat* in NOMPC localization. We found that *dTat* mutant c3da neurons exhibit normal NOMPC-GFP distribution when NOMPC-GFP is ectopically expressed (Figure 6A), suggesting that *dTat* regulates NOMPC function instead of localization. Second, NOMPC-microtubule interactions are critical to NOMPC function (Zhang et al., 2015); thus, we investigated *dTat* effects on NOMPC-microtubule

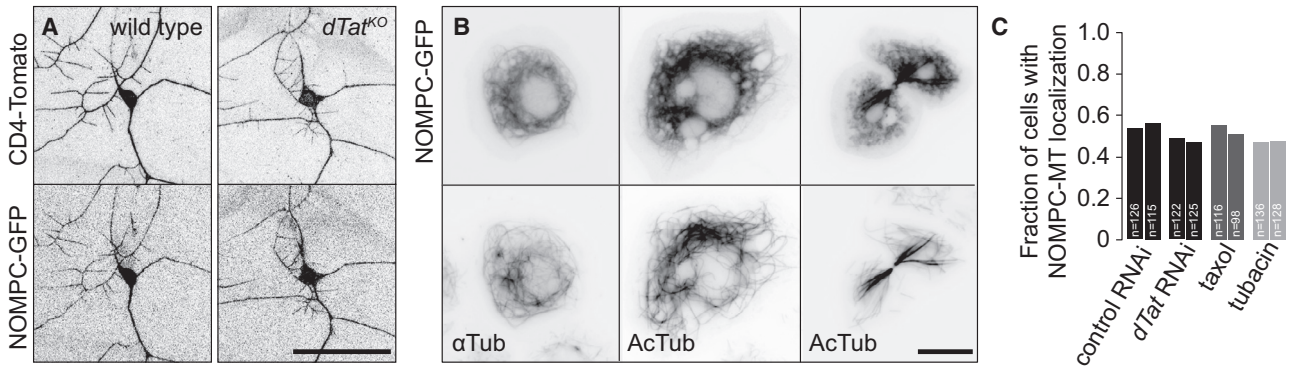

Figure 6. *dTat* Is Dispensable for NOMPC-Microtubule Interactions

(A) Maximum intensity projections showing GFP-NOMPC distribution in c3da neurons wild-type control (left) and $dTat^{KO}$ mutant (right) larvae additionally expressing the membrane marker CD4-tdTomato.

(B) S2 cells stably transfected with *UAS-GFP-nompC* were immunostained with antibodies to GFP and acTb or α-tubulin, as indicated. Images show cells in interphase (left, middle) and during anaphase (right).

(C) S2 cells stably transfected with *UAS-GFP-nompC* were treated with control RNAi, *dTat* RNAi, taxol, or tubacin; immunostained using GFP and tubulin antibodies; and the fraction of cells exhibiting NOMPC-microtubule co-localization was visually scored in a blind experiment. Chi-square tests revealed no differences in NOMPC-microtubule co-localization among the different treatments. The number of cells analyzed is shown for each treatment.

interactions in S2 cells. When expressed in S2 cells, NOMPC-GFP co-localizes with microtubules and is sufficient to confer mechanosensitivity to this normally non-responsive cell line (Yan et al., 2013). Although we found that NOMPC-GFP co-localized extensively with acTb (Figure 6B), neither eliminating microtubule acetylation with *dTat* RNAi (Figure 6C) nor treating S2 cells with the HDAC6 inhibitor tubacin or taxol to increase acTb levels significantly reduced NOMPC-GFP co-localization with microtubules, indicating that acTb is not a critical determinant of NOMPC-microtubule interactions.

dTAT Regulates Microtubule Breakage and/or Dynamics to Promote NOMPC-Dependent Mechanotransduction

Recent reports have established a role for acTb in regulating microtubule dynamics and in conferring microtubules with resistance to mechanical breakage (Portran et al., 2017; Xu et al., 2017). Because NOMPC interacts with microtubules via its AR domain and this interaction is required for mechanosensation (Cheng et al., 2010; Zhang et al., 2015), we speculated that loss of *dTat* would perturb the mechanical properties of microtubules and/or microtubule dynamics to inhibit mechanosensation. This hypothesis was supported by three independent lines of experimentation.

First, we examined microtubule plus end numbers and dynamics by expressing a GFP-tagged version of EB1 (*UAS-EB1-GFP*) in c3da neurons additionally expressing a membrane-targeted red fluorescent protein (*UAS-CD4-tdTomato*). In third instar larvae, *dTat* mutant c3da neurons exhibited a ~70% increase in EB1-GFP^+ puncta (control, 1.74 ± 0.51; *dTat* mutant, 2.99 ± 0.90) (Figures 7A–7E and S4). This increase in the number of growing plus ends could be caused by an increased rate of new microtubule nucleation events, destabilization of existing microtubules leading to increased rescue events, and periods of polymerization, or by increased frequency of microtubule breakage leading to the production of new plus ends (Goodwin and Vale, 2010). Next, we examined whether mechanical stimulus could alter microtubule plus end numbers by visualizing EB1-GFP puncta immediately before and after mechanical stimulus. We found that mechanical stimulus induced a significant increase in EB1-positive puncta in *dTat* mutant but not wild-type control c3da neurons (Figures 7F–7H). These results indicate that microtubule mechanical stability and/or dynamics are altered in *dTat* mutants compared to wild-type controls and that mechanical stimulus can trigger changes in the number of growing plus ends in the absence of microtubule acetylation.

Second, we examined the localization of the MAP1B-like protein, futsch. Futsch is required during *Drosophila* development for microtubule organization during axonal growth and synaptogenesis (Hummel et al., 2000; Roos et al., 2000). As a microtubule-associated protein, futsch has been used as a marker for microtubule polymer and an indicator of microtubule stability (Jenkins et al., 2017; Ruiz-Canada et al., 2004). Consistent with a role for acTb in regulating microtubule dynamics or stability, we observed a significant reduction in futsch immunoreactivity in c3da neurons of $dTat^{KO}$ or *αTub84B* mutants compared to wild-type controls (Figure S5); non-acetylatable *αTub84B* mutants similarly reduce futsch immunoreactivity in other da neurons (Jenkins et al., 2017). These results confirm that loss of acTb alters composition of the microtubule cytoskeleton in c3da neurons and potentially its stability.

Third, we examined whether taxol-mediated microtubule stabilization could potentiate mechanosensory responses. We found that acute taxol feeding led to dose-dependent increases in gentle-touch sensitivity in third-instar larvae over a range of 0–60 μM taxol (Figure 7I) with no obvious effects on neuron morphology (c3da neuron dendrite length, mean ± SD: 4.84 ± 0.76 mm, DMSO fed; 4.69 ± 0.88 mm, 60 μM taxol fed; n = 8 neurons each). Mutation of *nompC* rendered taxol-fed larvae insensitive to gentle touch as did c3da neuron-specific expression of

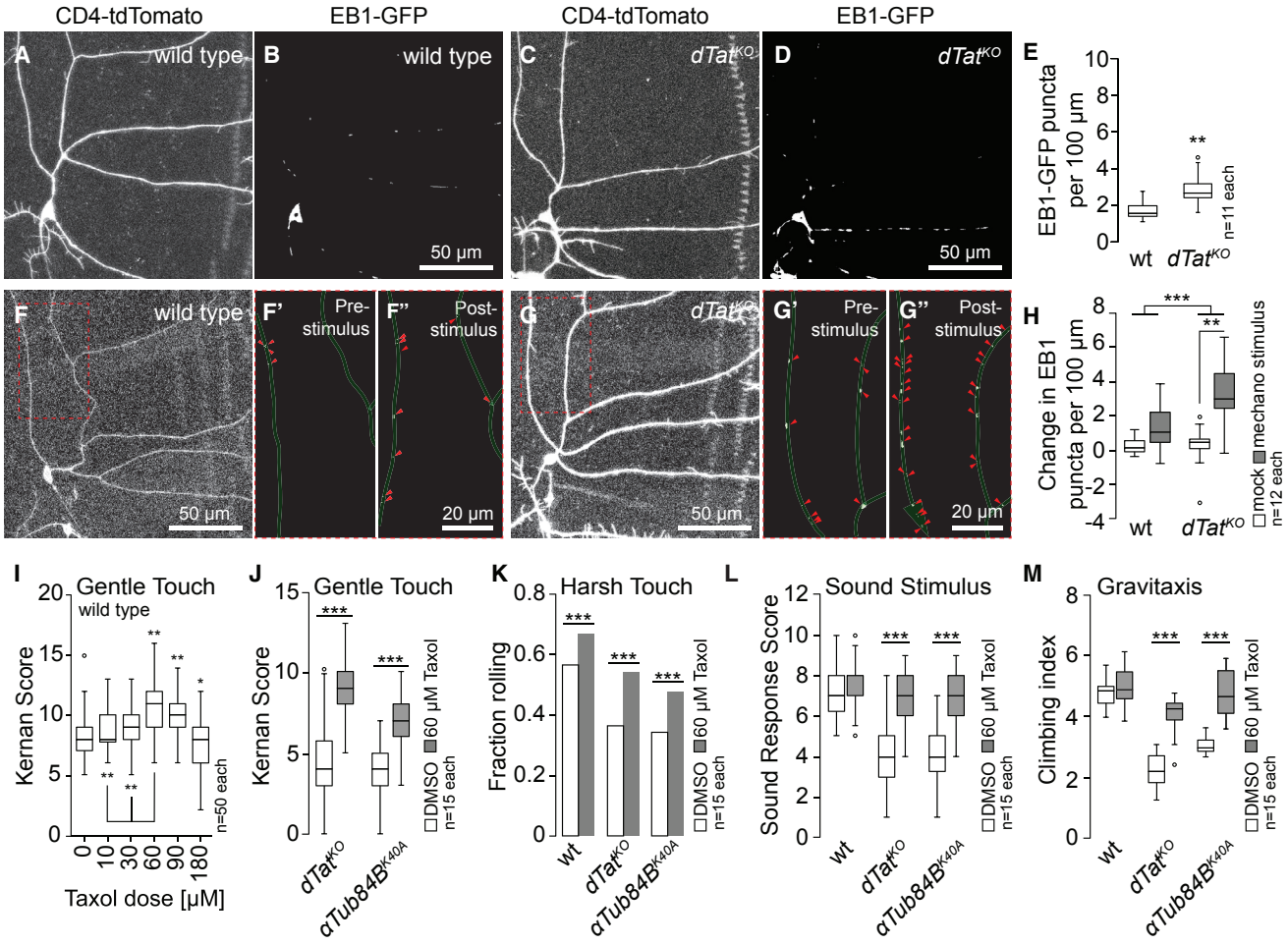

Figure 7. *dTat* Promotion of Microtubule Stability Modulates Mechanotransduction

(A–D) Representative images of c3da neurons from (A and B) wild-type (CD4-tdTomato, A; EB1-GFP, B) and (C and D) $dTat^{KO}$ mutant larvae expressing CD4-tdTomato to label membranes (C) and EB1-GFP to label microtubule plus ends (D).

(E) Boxplot depicts the number of $EB1^{+}$ puncta per 100 mm of dendrite length. $^{**}p < 0.01$ compared to wild-type; unpaired t test with Welch's correction.

(F–H) Microtubules of $dTat^{KO}$ mutants are prone to mechanically -induced breakage. Images of representative (F) wild-type and (G) *dTat* mutant c3da neurons that were subjected to mechanical stimulus are shown. EB1-GFP labeling is shown immediately before (F' and G') and after stimulus (F'' and G''). Arrowheads mark EB1 puncta.

(H) Boxplot depicting quantification of $EB1^{+}$ puncta. Two-way ANOVA analysis revealed a significant interaction effect between mechanical treatment and genotype on EB1 puncta number. $F(2,12) = 7.539$, $p = 0.009$. Simple main effects analysis showed a significant difference in EB1 puncta number between treated and untreated *dTat* mutant larvae ($p = 0.001$), but not between treated and untreated wild-type larvae ($p = 0.184$). $^{**}p < 0.01$, $^{***}p < 0.001$. Raw images are shown in Figure S4.

(I–M) Taxol-induced microtubule stabilization rescues mechanosensory defects of acetylation mutants.

(I) Boxplot depicting gentle touch response of larvae fed the indicated dose of taxol for 3 hr. $^{*}p < 0.05$, $^{**}p < 0.01$, compared to vehicle-fed controls; one-way ANOVA with a post hoc Dunnett's test.

(J) Boxplot depicting gentle touch response of *dTat* and *αTub84b* mutant larvae fed vehicle or 60 µM taxol for 3 hr.

(K) Bars depict the proportion of larvae of the indicated genotype that exhibited a nociceptive rolling responded to 44 mN von Frey stimulus.

(L and M) Boxplots depicting sound stimulus responses (L) and gravitaxis behavior (M) of wild-type, *dTat*, and *αTub84B* mutant flies fed vehicle or 60 µM taxol for 12 hr.

$^{***}p < 0.001$ compared to vehicle controls; unpaired t test with Welch's correction for (J–M). The number of independent samples measured for each genotype is shown in each panel.

See also Figures S4, S5, S6, and S7, and Table S2.

tetanus toxin (Figure S6), indicating that the increased responses to gentle touch require *nompC* and reflect enhanced activity of c3da neurons. To test whether mechanosensory defects of $dTat^{KO}$ and non-acetylatable $\alpha Tub84B^{K40A}$ mutants reflect a decrease in microtubule stability, we treated larvae with vehicle or 60 µM taxol and measured behavioral responses to gentle touch (Figure 7J). Remarkably, taxol feeding significantly enhanced gentle touch responses of $dTat^{KO}$ and $\alpha Tub84B^{K40A}$

mutants. Likewise, taxol feeding potentiated responses of wild-type larvae to harsh touch and significantly enhanced harsh touch responses of $dTat^{KO}$ and $\alpha Tub84B^{K40A}$ mutants (Figure 7K). Finally, although taxol feeding did not enhance vibration responses or gravitaxis in wild-type controls, it did restore these behaviors to wild-type levels in $dTat^{KO}$ and $\alpha Tub84B^{K40A}$ mutants (Figures 7L and 7M).

dTAT Regulates the Rigidity of Cultured S2 Cells

Our studies thus far support a model in which microtubule acetylation by *dTat* broadly regulates mechanosensation via effects on microtubule stability. We next examined whether dTAT regulates cellular rigidity, which could contribute to *dTat* mutant mechanosensation defects. Loss of the microtubule acetylase α-tubulin *N*-acetyltransferase 1 (ATAT1) results in increased cellular rigidity of cultured mouse DRG neurons (Morley et al., 2016). To test whether this biophysical function was conserved in *Drosophila*, we used atomic force microscopy (AFM) to examine the elastic moduli of dTAT-depleted S2 cells and compared them to control-treated cells. We found that *dTat* RNAi-treated cells exhibited a statistically significant increase in cortical stiffness, with *dTat* RNAi cells exhibiting a 22% increase in stiffness (Figure S7; Table S2). These results indicate that the role of dTAT/ATAT1 in regulating the mechanical properties of cells is conserved; whether this activity contributes to its role in mechanosensation remains to be determined.

DISCUSSION

Microtubule acetylation is required for touch sensation in several model systems (Akella et al., 2010; Morley et al., 2016); however, the molecular mechanisms that underlie its role in mechanosensation are poorly understood. In this study, we identified the major αTAT in *Drosophila*, dTAT, and found that it is broadly required for mechanosensation. In response to gentle touch, *dTat* functions in the same pathway as the TRP channel *nompC* and is required for NOMPC-dependent touch-evoked neuronal responses. *dTat* mutation causes an increase in dendritic microtubule plus ends in mechanosensory neurons, and taxol stabilization of the microtubule cytoskeleton rescues mechanoreceptivity, suggesting that microtubule breakage and/or alterations in microtubule dynamics underlie the loss of touch sensitivity. We also observed that dTAT depletion in S2 cells altered their mechanical properties to make them more rigid, an effect that could alter NOMPC activation in neurons by increasing its threshold for activation. Collectively, our results suggest that K40 acetylation functions to stabilize the microtubule cytoskeleton and may tune cellular mechanics to promote NOMPC activation through its cytoplasmic microtubule-associated tension gate. Our results demonstrating defects in vibration perception and gravitaxis in *dTat* mutants reveal that microtubule acetylation plays a broader role in mechanosensation than was previously recognized. We speculate that microtubule acetylation likewise promotes the activation of other mechanosensory channels by facilitating microtubule-mediated mechanotransduction.

The results of our genetic, electrophysiological, and cell biological experiments indicate that *dTat* is required for mechanosensation by the TRP channel NOMPC. This requirement is not related to NOMPC trafficking and unlikely due to interactions with microtubules. Instead, we observed an increase in EB1-labeled microtubule plus ends in *dTat* mutant sensory dendrites and showed that stabilizing the cytoskeleton by feeding mutant animals taxol rescued touch sensitivity. In light of recent findings that K40 acetylation weakened inter-protofilament interactions, allowing microtubules to comply with deformative forces without breaking (Portran et al., 2017; Xu et al., 2017), our results suggest that in the absence of K40 acetylation, microtubules in c3da neurons are mechanically damaged, thereby decreasing NOMPC-microtubule interactions and attenuating the channel's ability to transduce mechanical stimuli. We cannot exclude the possibility that regulation of microtubule dynamics is a major functional role for acetylation in PNS neurons; further investigation into the influence of microtubule structure and dynamics on NOMPC-microtubule interactions should help resolve whether acetylation controls mechanosensation primarily via the regulation of microtubule mechanical resilience or dynamics.

Loss of *dTat* does not phenocopy *nompC* null mutants in all respects. NOMPC functions in proprioceptive c1da neurons to control larval locomotion (Cheng et al., 2010), but *dTat* mutant larvae exhibit grossly normal locomotion. Although the absence of obvious defects in our assay does not preclude the possibility that *dTat* exerts a subtle influence on larval locomotion, the effects of *dTat* mutation are significantly less pronounced than the ~50% decrease in larval crawling speed observed in *nompC* mutants (Cheng et al., 2010). We speculate that this may be due to neuron class-specific susceptibility to the loss of acTb. For example, the microtubule network in c1da neurons may be more resistant to loss of *dTat* than in c4da neurons. We also discovered that adult gravitaxis is perturbed in *dTat* mutants. While NOMPC is dispensable for gravitaxis, TRPA and TRPV family channels are required for gravity sensing (Kamikouchi et al., 2009; Sun et al., 2009). Likewise, *dTat* mutants have defects in harsh touch responses, which involve TRP, piezo, and Ppk/ENaC channels but not NOMPC, as well as defects in larval hearing, which involve several TRP channels in addition to NOMPC. These results raise the possibility that interactions between acTb and other channels may play important roles in mechanosensation.

Prior studies of microtubule acetylation in touch perception have arrived at molecular mechanisms that differ from our model but are not mutually exclusive. In *C. elegans* touch receptor neurons, sensory dendrites are packed with a cross-linked bundle of long, specialized 15-protofilament microtubules specific to this cell type (Chalfie and Sulston, 1981). Mutation of the αTATs *mec-17* and *atat-2* resulted in the loss of these unique microtubules and insensitivity to touch (Bounoutas et al., 2009). Thus, K40 acetylation is required for the assembly of a specialized population of microtubules involved in *C. elegans* mechanotransduction. Although there is no evidence for specialized microtubules in *Drosophila* da neuron dendrites, the results from worm touch receptors mirror our results in that microtubule acetylation is required to maintain an intact microtubule network. Further electron microscopy (EM) study of the cytoskeleton in da neurons will be necessary to definitively determine whether they possess specialized microtubule arrays.

In mouse peripheral sensory neurons, acetylated microtubules are enriched in a submembranous band in the soma that is

distinct from the cytoplasmic microtubule network (Morley et al., 2016). This submembranous band appears to confer rigidity to the plasma membrane, and cultured DRG neurons from *Atat1* knockout mice exhibited increased membrane stiffness (Morley et al., 2016). The authors proposed that in this system, microtubule acetylation tunes the mechanical properties of the membrane and, in its absence, cells are less elastic and require more force to trigger mechanosensitive channels. Our results in S2 cells indicate that regulation of cellular stiffness is a conserved function for microtubule acetylases. However, the molecular mechanism linking microtubule acetylation to cellular stiffness and the extent to which this alteration of cellular stiffness contributes to mechanosensation are unknown. To address these important outstanding issues, it will be necessary to identify the molecular components that link microtubules to the mechanical properties of the cell cortex and examine their contribution to mechanosensation independently of microtubule function. Although we have found no evidence for a specialized submembranous network of acetylated microtubules in *Drosophila* PNS neurons, it will be interesting to determine whether *dTat* regulates cellular elasticity in these cells as well. It is therefore possible that microtubule acetylation regulates mechanosensitivity through multiple mechanisms: by regulating microtubule structure and by tuning the mechanical properties of neurons.

STAR★METHODS

Detailed methods are provided in the online version of this paper and include the following:

- KEY RESOURCES TABLE
- CONTACT FOR REAGENT AND RESOURCE SHARING
- EXPERIMENTAL MODEL AND SUBJECT DETAILS
  - Fly husbandry
  - Fly stocks
  - Cell Culture
- METHOD DETAILS
  - Generation of *dTat* alleles
  - RNA-Seq of larval cells
  - Plasmid Constructs
  - Identification of candidate *Drosophila* acetylases
  - S2 cell culture, RNAi, and immunofluorescence
  - Antibodies
  - Imaging of larval samples
  - Behavior assays
  - Electrophysiology
  - Atomic force microscope measurements
- QUANTIFICATION AND STATISTICAL ANALYSIS
- DATA AND SOFTWARE AVAILABILITY

SUPPLEMENTAL INFORMATION

Supplemental Information includes seven figures and four tables and can be found with this article online at https://doi.org/10.1016/j.celrep.2018.09.075.

ACKNOWLEDGMENTS

This work was supported by a grant from the NIH/National Institute of Neurological Disorders and Stroke (NINDS) (R01NS076614), a University of Washington Research Innovation award, and startup funds from the University of Washington to J.Z.P.; support from Mark Peifer and a University of North Carolina Biology/iBGS Pilot Award to S.L.R.; grants from the NIH/NINDS (R01NS089787 and R21NS107924) to Y.X.; a grant from the NIH/NINDS (R21NS101553) to J.W.; a Klingenstein-Simons Fellowship to J.C.T.; a grant from the NIH/National Institute of Biomedical Imaging and Bioengineering (NIBIB) (5-P41-EB002025-33) to R.S.; and a grant from the NIH/National Institute of Mental Health (NIMH) (R01MH115767) to J.C.V. Fly stocks obtained from the Bloomington *Drosophila* Stock Center (NIH P40OD018537) and antibodies from the Developmental Studies Hybridoma Bank, created by the Eunice Kennedy Shriver National Institute of Child Health and Human Development (NICHD) of the NIH and maintained at The University of Iowa, were used in this study. We thank Mark Peifer and Peter Soba for critical reading of this manuscript.

AUTHOR CONTRIBUTIONS

C.Y. performed and analyzed the larval imaging and behavior assays and generated the transgenic lines. F.W. and Y.X. performed and analyzed the calcium imaging assays. Y.P. generated the *dTat* CRISPR alleles. C.R.W. performed the RNA-seq analysis. B.J. and J.W. contributed the α*Tub84b* alleles. C.Y., H.-J.K., J.B.P. and J.C.V. performed the expansion microscopy. M.E.K., M.R.F., E.T.O., and R.S. performed and analyzed the AFM assays. J.C.T. performed and analyzed the electrophysiology assays. S.L.R. performed the S2 cell assays. S.L.R. and J.Z.P. designed and supervised the project, analyzed the data, and wrote the manuscript.

DECLARATION OF INTERESTS

The authors declare no competing interests.

Received: January 22, 2018
Revised: August 4, 2018
Accepted: September 24, 2018
Published: October 23, 2018

REFERENCES

Ageta-Ishihara, N., Miyata, T., Ohshima, C., Watanabe, M., Sato, Y., Hamamura, Y., Higashiyama, T., Mazitschek, R., Bito, H., and Kinoshita, M. (2013). Septins promote dendrite and axon development by negatively regulating microtubule stability via HDAC6-mediated deacetylation. Nat. Commun. *4*, 2532.

Akella, J.S., Wloga, D., Kim, J., Starostina, N.G., Lyons-Abbott, S., Morrissette, N.S., Dougan, S.T., Kipreos, E.T., and Gaertig, J. (2010). MEC-17 is an alpha-tubulin acetyltransferase. Nature *467*, 218–222.

Baek, M., and Mann, R.S. (2009). Lineage and birth date specify motor neuron targeting and dendritic architecture in adult Drosophila. J. Neurosci. *29*, 6904–6916.

Beicker, K., O'Brien, E.T., 3rd, Falvo, M.R., and Superfine, R. (2018). Vertical light sheet enhanced side-view imaging for AFM cell mechanics studies. Sci. Rep. *8*, 1504.

Bhuwania, R., Castro-Castro, A., and Linder, S. (2014). Microtubule acetylation regulates dynamics of KIF1C-powered vesicles and contact of microtubule plus ends with podosomes. Eur. J. Cell Biol. *93*, 424–437.

Boiko, N., Medrano, G., Montano, E., Jiang, N., Williams, C.R., Madungwe, N.B., Bopassa, J.C., Kim, C.C., Parrish, J.Z., Hargreaves, K.M., et al. (2017). TrpA1 activation in peripheral sensory neurons underlies the ionic basis of pain hypersensitivity in response to vinca alkaloids. PLoS One *12*, e0186888.

Bounoutas, A., O'Hagan, R., and Chalfie, M. (2009). The multipurpose 15-protofilament microtubules in C. elegans have specific roles in mechanosensation. Curr. Biol. *19*, 1362–1367.

Branson, K., Robie, A., Bender, J., Perona, P., and Dickinson, M. (2009). High-throughput ethomics in large groups of Drosophila. Nat. Methods *6*, 451–457.

Brierley, D.J., Rathore, K., VijayRaghavan, K., and Williams, D.W. (2012). Developmental origins and architecture of Drosophila leg motoneurons. J. Comp. Neurol. *520*, 1629–1649.

Chalfie, M., and Au, M. (1989). Genetic control of differentiation of the Caenorhabditis elegans touch receptor neurons. Science *243*, 1027–1033.

Chalfie, M., and Sulston, J. (1981). Developmental genetics of the mechanosensory neurons of Caenorhabditis elegans. Dev. Biol. *82*, 358–370.

Chattopadhyay, A., Gilstrap, A.V., and Galko, M.J. (2012). Local and global methods of assessing thermal nociception in Drosophila larvae. J. Vis. Exp. *63*, e3837.

Cheng, L.E., Song, W., Looger, L.L., Jan, L.Y., and Jan, Y.N. (2010). The role of the TRP channel NompC in Drosophila larval and adult locomotion. Neuron *67*, 373–380.

Christensen, A.P., and Corey, D.P. (2007). TRP channels in mechanosensation: direct or indirect activation? Nat. Rev. Neurosci. *8*, 510–521.

Conacci-Sorrell, M., Ngouenet, C., and Eisenman, R.N. (2010). Myc-nick: a cytoplasmic cleavage product of Myc that promotes alpha-tubulin acetylation and cell differentiation. Cell *142*, 480–493.

Coste, B., Mathur, J., Schmidt, M., Earley, T.J., Ranade, S., Petrus, M.J., Dubin, A.E., and Patapoutian, A. (2010). Piezo1 and Piezo2 are essential components of distinct mechanically activated cation channels. Science *330*, 55–60.

Creppe, C., Malinouskaya, L., Volvert, M.-L., Gillard, M., Close, P., Malaise, O., Laguesse, S., Cornez, I., Rahmouni, S., Ormenese, S., et al. (2009). Elongator controls the migration and differentiation of cortical neurons through acetylation of alpha-tubulin. Cell *136*, 551–564.

Cribb, J.A., Osborne, L.D., Beicker, K., Psioda, M., Chen, J., O'Brien, E.T., Taylor Ii, R.M., Vicci, L., Hsiao, J.P.-L., Shao, C., et al. (2016). An automated high-throughput array microscope for cancer cell mechanics. Sci. Rep. *6*, 27371.

Dobin, A., Davis, C.A., Schlesinger, F., Drenkow, J., Zaleski, C., Jha, S., Batut, P., Chaisson, M., and Gingeras, T.R. (2013). STAR: ultrafast universal RNA-seq aligner. Bioinformatics *29*, 15–21.

Gong, J., Wang, Q., and Wang, Z. (2013). NOMPC is likely a key component of Drosophila mechanotransduction channels. Eur. J. Neurosci. *38*, 2057–2064.

Goodwin, S.S., and Vale, R.D. (2010). Patronin regulates the microtubule network by protecting microtubule minus ends. Cell *143*, 263–274.

Gouwens, N.W., and Wilson, R.I. (2009). Signal propagation in Drosophila central neurons. J. Neurosci. *29*, 6239–6249.

Gratz, S.J., Ukken, F.P., Rubinstein, C.D., Thiede, G., Donohue, L.K., Cummings, A.M., and O'Connor-Giles, K.M. (2014). Highly specific and efficient CRISPR/Cas9-catalyzed homology-directed repair in Drosophila. Genetics *196*, 961–971.

Grubbs, F.E. (1950). Sample criteria for testing outlying observations. Ann. Math. Stat. *21*, 27–58.

Han, C., Jan, L.Y., and Jan, Y.-N. (2011). Enhancer-driven membrane markers for analysis of nonautonomous mechanisms reveal neuron-glia interactions in Drosophila. Proc. Natl. Acad. Sci. USA *108*, 9673–9678.

Howard, J., and Bechstedt, S. (2004). Hypothesis: a helix of ankyrin repeats of the NOMPC-TRP ion channel is the gating spring of mechanoreceptors. Curr. Biol. *14*, R224–R226.

Howard, J., and Hudspeth, A.J. (1987). Mechanical relaxation of the hair bundle mediates adaptation in mechanoelectrical transduction by the bullfrog's saccular hair cell. Proc. Natl. Acad. Sci. USA *84*, 3064–3068.

Hubbert, C., Guardiola, A., Shao, R., Kawaguchi, Y., Ito, A., Nixon, A., Yoshida, M., Wang, X.-F., and Yao, T.-P. (2002). HDAC6 is a microtubule-associated deacetylase. Nature *417*, 455–458.

Hummel, T., Krukkert, K., Roos, J., Davis, G., and Klämbt, C. (2000). Drosophila Futsch/22C10 is a MAP1B-like protein required for dendritic and axonal development. Neuron *26*, 357–370.

Hwang, R.Y., Zhong, L., Xu, Y., Johnson, T., Zhang, F., Deisseroth, K., and Tracey, W.D. (2007). Nociceptive neurons protect Drosophila larvae from parasitoid wasps. Curr. Biol. *17*, 2105–2116.

Jenkins, B.V., Saunders, H.A.J., Record, H.L., Johnson-Schlitz, D.M., and Wildonger, J. (2017). Effects of mutating α-tubulin lysine 40 on sensory dendrite development. J. Cell Sci. *130*, 4120–4131.

Jiang, N., Kim, H.-J., Chozinski, T.J., Azpurua, J.E., Eaton, B.A., Vaughan, J.C., and Parrish, J.Z. (2018). Superresolution imaging of Drosophila tissues using expansion microscopy. Mol. Biol. Cell *29*, 1413–1421.

Jiang, N., Soba, P., Parker, E., Kim, C.C., and Parrish, J.Z. (2014). The microRNA bantam regulates a developmental transition in epithelial cells that restricts sensory dendrite growth. Dev. Camb. Engl *141*, 2657–2668.

Jin, P., Bulkley, D., Guo, Y., Zhang, W., Guo, Z., Huynh, W., Wu, S., Meltzer, S., Cheng, T., Jan, L.Y., et al. (2017). Electron cryo-microscopy structure of the mechanotransduction channel NOMPC. Nature *547*, 118–122.

Kalebic, N., Martinez, C., Perlas, E., Hublitz, P., Bilbao-Cortes, D., Fiedorczuk, K., Andolfo, A., and Heppenstall, P.A. (2013a). Tubulin acetyltransferase αTAT1 destabilizes microtubules independently of its acetylation activity. Mol. Cell. Biol. *33*, 1114–1123.

Kalebic, N., Sorrentino, S., Perlas, E., Bolasco, G., Martinez, C., and Heppenstall, P.A. (2013b). αTAT1 is the major α-tubulin acetyltransferase in mice. Nat. Commun. *4*, 1962.

Kamikouchi, A., Inagaki, H.K., Effertz, T., Hendrich, O., Fiala, A., Göpfert, M.C., and Ito, K. (2009). The neural basis of Drosophila gravity-sensing and hearing. Nature *458*, 165–171.

Kaneko, T., Macara, A.M., Li, R., Hu, Y., Iwasaki, K., Dunnings, Z., Firestone, E., Horvatic, S., Guntur, A., Shafer, O.T., et al. (2017). Serotonergic modulation enables pathway-specific plasticity in a developing sensory circuit in Drosophila. Neuron *95*, 623–638.e4.

Katta, S., Krieg, M., and Goodman, M.B. (2015). Feeling force: physical and physiological principles enabling sensory mechanotransduction. Annu. Rev. Cell Dev. Biol. *31*, 347–371.

Kernan, M., Cowan, D., and Zuker, C. (1994). Genetic dissection of mechanosensory transduction: mechanoreception-defective mutations of Drosophila. Neuron *12*, 1195–1206.

Kim, G.-W., Li, L., Ghorbani, M., You, L., and Yang, X.-J. (2013). Mice lacking α-tubulin acetyltransferase 1 are viable but display α-tubulin acetylation deficiency and dentate gyrus distortion. J. Biol. Chem. *288*, 20334–20350.

Kung, C. (2005). A possible unifying principle for mechanosensation. Nature *436*, 647–654.

L'Hernault, S.W., and Rosenbaum, J.L. (1985). Chlamydomonas alpha-tubulin is posttranslationally modified by acetylation on the epsilon-amino group of a lysine. Biochemistry *24*, 473–478.

Liang, X., Madrid, J., Gärtner, R., Verbavatz, J.-M., Schiklenk, C., Wilsch-Bräuninger, M., Bogdanova, A., Stenger, F., Voigt, A., and Howard, J. (2013). A NOMPC-dependent membrane-microtubule connector is a candidate for the gating spring in fly mechanoreceptors. Curr. Biol. *23*, 755–763.

Morley, S.J., Qi, Y., Iovino, L., Andolfi, L., Guo, D., Kalebic, N., Castaldi, L., Tischer, C., Portulano, C., Bolasco, G., et al. (2016). Acetylated tubulin is essential for touch sensation in mice. eLife *5*, e20813.

North, B.J., Marshall, B.L., Borra, M.T., Denu, J.M., and Verdin, E. (2003). The human Sir2 ortholog, SIRT2, is an NAD+-dependent tubulin deacetylase. Mol. Cell *11*, 437–444.

O'Hagan, R., Chalfie, M., and Goodman, M.B. (2005). The MEC-4 DEG/ENaC channel of Caenorhabditis elegans touch receptor neurons transduces mechanical signals. Nat. Neurosci. *8*, 43–50.

Ohkawa, N., Sugisaki, S., Tokunaga, E., Fujitani, K., Hayasaka, T., Setou, M., and Inokuchi, K. (2008). N-acetyltransferase ARD1-NAT1 regulates neuronal dendritic development. Genes Cells *13*, 1171–1183.

Park, I.Y., Powell, R.T., Tripathi, D.N., Dere, R., Ho, T.H., Blasius, T.L., Chiang, Y.-C., Davis, I.J., Fahey, C.C., Hacker, K.E., et al. (2016). Dual chromatin and cytoskeletal remodeling by SETD2. Cell *166*, 950–962.

Patro, R., Duggal, G., Love, M.I., Irizarry, R.A., and Kingsford, C. (2017). Salmon provides fast and bias-aware quantification of transcript expression. Nat. Methods *14*, 417–419.

Petersen, L.K., and Stowers, R.S. (2011). A Gateway MultiSite recombination cloning toolkit. PLoS One *6*, e24531.

Portran, D., Schaedel, L., Xu, Z., Théry, M., and Nachury, M.V. (2017). Tubulin acetylation protects long-lived microtubules against mechanical ageing. Nat. Cell Biol. *19*, 391–398.

Prager-Khoutorsky, M., Khoutorsky, A., and Bourque, C.W. (2014). Unique interweaved microtubule scaffold mediates osmosensory transduction via physical interaction with TRPV1. Neuron *83*, 866–878.

Reed, N.A., Cai, D., Blasius, T.L., Jih, G.T., Meyhofer, E., Gaertig, J., and Verhey, K.J. (2006). Microtubule acetylation promotes kinesin-1 binding and transport. Curr. Biol. *16*, 2166–2172.

Rogers, S.L., and Rogers, G.C. (2008). Culture of Drosophila S2 cells and their use for RNAi-mediated loss-of-function studies and immunofluorescence microscopy. Nat. Protoc. *3*, 606–611.

Roos, J., Hummel, T., Ng, N., Klämbt, C., and Davis, G.W. (2000). Drosophila Futsch regulates synaptic microtubule organization and is necessary for synaptic growth. Neuron *26*, 371–382.

Ruiz-Canada, C., Ashley, J., Moeckel-Cole, S., Drier, E., Yin, J., and Budnik, V. (2004). New synaptic bouton formation is disrupted by misregulation of microtubule stability in aPKC mutants. Neuron *42*, 567–580.

Schindelin, J., Arganda-Carreras, I., Frise, E., Kaynig, V., Longair, M., Pietzsch, T., Preibisch, S., Rueden, C., Saalfeld, S., Schmid, B., et al. (2012). Fiji: an open-source platform for biological-image analysis. Nat. Methods *9*, 676–682.

Shida, T., Cueva, J.G., Xu, Z., Goodman, M.B., and Nachury, M.V. (2010). The major alpha-tubulin K40 acetyltransferase alphaTAT1 promotes rapid ciliogenesis and efficient mechanosensation. Proc. Natl. Acad. Sci. USA *107*, 21517–21522.

Song, W., Onishi, M., Jan, L.Y., and Jan, Y.N. (2007). Peripheral multidendritic sensory neurons are necessary for rhythmic locomotion behavior in Drosophila larvae. Proc. Natl. Acad. Sci. U.S.A *104*, 5199–5204.

Sudo, H., and Baas, P.W. (2010). Acetylation of microtubules influences their sensitivity to severing by katanin in neurons and fibroblasts. J. Neurosci. *30*, 7215–7226.

Sun, Y., Liu, L., Ben-Shahar, Y., Jacobs, J.S., Eberl, D.F., and Welsh, M.J. (2009). TRPA channels distinguish gravity sensing from hearing in Johnston's organ. Proc. Natl. Acad. Sci. USA *106*, 13606–13611.

Szyk, A., Deaconescu, A.M., Spector, J., Goodman, B., Valenstein, M.L., Ziolkowska, N.E., Kormendi, V., Grigorieff, N., and Roll-Mecak, A. (2014). Molecular basis for age-dependent microtubule acetylation by tubulin acetyltransferase. Cell *157*, 1405–1415.

Tanner, K.D., Levine, J.D., and Topp, K.S. (1998). Microtubule disorientation and axonal swelling in unmyelinated sensory axons during vincristine-induced painful neuropathy in rat. J. Comp. Neurol. *395*, 481–492.

Topalidou, I., Keller, C., Kalebic, N., Nguyen, K.C.Q., Somhegyi, H., Politi, K.A., Heppenstall, P., Hall, D.H., and Chalfie, M. (2012). Genetically separable functions of the MEC-17 tubulin acetyltransferase affect microtubule organization. Curr. Biol. *22*, 1057–1065.

Tsubouchi, A., Caldwell, J.C., and Tracey, W.D. (2012). Dendritic filopodia, Ripped Pocket, NOMPC, and NMDARs contribute to the sense of touch in Drosophila larvae. Curr. Biol. *22*, 2124–2134.

Tuthill, J.C., and Wilson, R.I. (2016). Parallel transformation of tactile signals in central circuits of Drosophila. Cell *164*, 1046–1059.

Walker, R.G., Willingham, A.T., and Zuker, C.S. (2000). A Drosophila mechanosensory transduction channel. Science *287*, 2229–2234.

Williams, C.R., Baccarella, A., Parrish, J.Z., and Kim, C.C. (2016). Trimming of sequence reads alters RNA-Seq gene expression estimates. BMC Bioinformatics *17*, 103.

Xiang, Y., Yuan, Q., Vogt, N., Looger, L.L., Jan, L.Y., and Jan, Y.N. (2010). Light-avoidance-mediating photoreceptors tile the Drosophila larval body wall. Nature *468*, 921–926.

Xu, Z., Schaedel, L., Portran, D., Aguilar, A., Gaillard, J., Marinkovich, M.P., Théry, M., and Nachury, M.V. (2017). Microtubules acquire resistance from mechanical breakage through intralumenal acetylation. Science *356*, 328–332.

Yan, Z., Zhang, W., He, Y., Gorczyca, D., Xiang, Y., Cheng, L.E., Meltzer, S., Jan, L.Y., and Jan, Y.N. (2013). Drosophila NOMPC is a mechanotransduction channel subunit for gentle-touch sensation. Nature *493*, 221–225.

Zhang, W., Yan, Z., Jan, L.Y., and Jan, Y.N. (2013). Sound response mediated by the TRP channels NOMPC, NANCHUNG, and INACTIVE in chordotonal organs of Drosophila larvae. Proc. Natl. Acad. Sci. USA *110*, 13612–13617.

Zhang, W., Cheng, L.E., Kittelmann, M., Li, J., Petkovic, M., Cheng, T., Jin, P., Guo, Z., Göpfert, M.C., Jan, L.Y., and Jan, Y.N. (2015). Ankyrin repeats convey force to gate the NOMPC mechanotransduction channel. Cell *162*, 1391–1403.

Zhong, L., Hwang, R.Y., and Tracey, W.D. (2010). Pickpocket is a DEG/ENaC protein required for mechanical nociception in Drosophila larvae. Curr. Biol. *20*, 429–434.

STAR★METHODS

KEY RESOURCES TABLE

REAGENT or RESOURCE	SOURCE	IDENTIFIER
Antibodies		
Mouse monoclonal anti-Tubulin (clone DM1A)	Sigma-Aldrich	Cat# T9026; RRID: AB_477593
Mouse monoclonal anti-Tubulin (clone 6-11B-1)	Sigma-Aldrich	Cat#T7451, RRID: AB_609894
Mouse monoclonal anti-Tubulin (clone DM1A); FITC conjugate	Sigma-Aldrich	Cat# F2168, RRID: AB_476967
Mouse monoclonal anti-Myc (clone 9E10)	Developmental Studies Hybridoma Bank (DSHB)	Cat# 9E 10, RRID: AB_2266850
Mouse monoclonal anti-Futsch (clone 22C10)	DSHB	Cat# 22c10, RRID: AB_528403
Rabbit polyclonal anti-GFP antibody	Fisher	Cat# A-11122, RRID: AB_22159
Rabbit polyclonal anti-dsRed antibody	Clontech	Cat# 632496, RRID: AB_10013483
Rabbit polyclonal anti-dTat antibody	This study	N/A
Chemicals, Peptides, and Recombinant Proteins		
Paclitaxel	Sigma-Aldrich	T7402
Tubacin	Sigma-Aldrich	SML0065
Deposited Data		
D. melanogaster larval PNS RNA-Seq data	Williams et al., 2016	NCBI-SRA GSE72884
D. melanogaster whole larva RNA-Seq data	Boiko et al., 2017	NCBI-SRA GSE99711
D. melanogaster larval cell type RNA-Seq data	This study	NCBI-SRA GSE120305
Experimental Models: Cell Lines		
D. melanogaster: Cell line S2	Derosophila Genomics Resource Center	S2-DGRC
Experimental Models: Organisms/Strains		
w[1118] ; dTat[KO]	This study	NA
w[1118] ; dTat[GFP]	This study	NA
w[1118] ; UAS-GFP-dTat-L	This study	NA
y[1] M{vas-Cas9.RFP-}ZH-2A w[1118]/FM7a, P{w[+mC] = Tb[1]}FM7-A	Bloomington Drosophila Stock Center (BDSC)	55821
y[1] w[67c23] P{y[+mDint2] = Crey}1b; sna[Sco]/CyO; Dr[1]/TM3, Sb[1]	BDSC	34516
w[1118]	BDSC	6326
w[1118] ; ppk-Gal4	BDSC	32079
y[1] w[*] HDAC6[KO]	BDSC	51182
nompC[1] cn[1] bw[1]/CyO	BDSC	42268
nompC[3] cn[1] bw[1]/CyO	BDSC	42258
w[1118]; P{w[+mC] = AyGAL4}17b	BDSC	4413
y[1] w[*]; PBac{y[+mDint2] w[+mC] = nompC-GAL4.P}VK00014; Df(3L)Ly, sens[Ly-1]/TM6C, Sb[1] Tb[1]	BDSC	36361
w[*]; P{w[+mC] = UAS-TeTxLC.tnt}R3	BDSC	28997
w; P{UAS-Hsap＼KCNJ2.EGFP}7*	BDSC	6595
w[*]; M{w[+mC] = UAS-Kat60.M}ZH-51D/CyO	BDSC	64117
w[1118]; P{w[+mC] = UAS-Eb1.EGFP.H}G	BDSC	36861
y[1] w[*]; P{w[+mC] = UAS-CD4-tdTom}7M1	BDSC	35841
w[1118]; P{w[+mC] = ppk-CD4-tdTom}10a/TM6B, Tb[1]	BDSC	35845
w[1118]; Df(3L)BSC113/TM6B, Tb[1]	BDSC	8970
w[1118], ppk-mCD8-GFP	Jiang et al., 2014	NA
w[1118] ; αTub84B[K40A]	Jenkins et al., 2017	NA
w[1118] ; αTub84B[K40R]	Jenkins et al., 2017	NA

(*Continued on next page*)

Continued		
REAGENT or RESOURCE	SOURCE	IDENTIFIER
w[1118] ; αTub84B[Δ]	Jenkins et al., 2017	NA
w[1118]; P{w[+mW.hs] = GawB}21-7	Song et al., 2007	NA
w[1118]; P{w[+mW.hs] = GawB}19-12	Xiang et al., 2010	NA
Oligonucleotides		
Oligonucleotide sequences used in this study are listed in Table S4.	This study	NA
Recombinant DNA		
pBID-UAS-GFP-dTat-L	This study	NA
pET28a dTat (1-196)	This study	NA
pMT B V5/His dTat(alt)-S	This study	NA
pMT B V5/His dTat(alt)-S GG (G133Y, G135Y)	This study	NA
pMT B V5/His dTat(alt)-S	This study	NA
pMT B V5/His dTat(alt)-L GG (G133Y, G135Y)	This study	NA

CONTACT FOR REAGENT AND RESOURCE SHARING

Further information and requests for resources and reagents should be directed to and will be fulfilled by the Lead Contact, Jay Parrish (jzp2@uw.edu).

EXPERIMENTAL MODEL AND SUBJECT DETAILS

Fly husbandry

Flies were maintained on standard cornmeal-molasses-agar media and reared at 25°C under 12 h alternating light-dark cycles.

Fly stocks

Alleles used in this study are listed in the Key Resources Table below and a complete list of experimental genotypes is available in Table S3.

Cell Culture

Culture and RNAi of *Drosophila* S2 cells were performed as previously described (Rogers and Rogers, 2008). S2 cells (*Drosophila* Genomics Resource Center, Bloomington, IN) were cultured in SF900II medium supplemented with 100x antibiotic-antimycotic (Invitrogen, Carlsbad, CA).

METHOD DETAILS

Generation of *dTat* alleles

The $dTat^{KO}$ and $dTat^{GFP}$ alleles were engineered using CRISPR/Cas9 mediated gene editing (Gratz et al., 2014). Target sites were selected upstream of the first coding exon and in the second intron of *dTat* using the CRISPR Optimal Target Finder (http://tools.flycrispr.molbio.wisc.edu/targetFinder/). chiRNA plasmids were generated by annealing sense and antisense gRNA oligos, digesting with BbsI, and ligating into the pU6-BbsI-chiRNA expression vector. Donor vectors were generated by cloning homology arms into pHD-DsRed. For $dTat^{KO}$, homology arms were designed to delete an 869 base pair fragment spanning the first three coding exons, beginning 16 base pairs upstream of the start codon. The donor vector for $dTat^{GFP}$ was generated as follows: pHD-dsRed was digested with EcoRI and the 5′ homology arm corresponding to sequences immediately upstreat of the *dTat* start codon, GFP and *dTat* PCR fragments were cloned into the backbone by Gibson assembly (NEB Gibson Assembly Kit) with GFP fused in-frame with the N terminus of *dTat* and the LoxP-flanked 3xP3-dsRed marker within the second intron. The newly assembled plasmid was then digested with XhoI and the 3′ homology arm was inserted using Gibson assembly. All primer sequences are available in Table S4.

chiRNA and pHD-DsRed plasmids were co-injected into embryos expressing Cas9 in the germline (BL55821: *y[1] M{vas-Cas9.RFP-}ZH-2A w[1118]/FM7a, P{w[+mC] = Tb[1]}FM7-A*), stocks were established from RFP-positive founder males, and 3xP3-RFP markers were removed using Cre-mediated reduction (BL34516: *y[1] w[67c23] P{y[+mDint2] = Crey}1b; sna[Sco]/CyO; Dr[1]/TM3, Sb[1]*) as previously described (Gratz et al., 2014).

RNA-Seq of larval cells

Four to seven samples of one hundred cells each were isolated and RNA-Seq libraries were prepared as described previously (Boiko et al., 2017). Briefly, third instar larvae expressing *UAS-Red Stinger* in the target cell type (epithelia, *a58-Gal4*; muscles, *mef-Gal4*;

peripheral neurons, *elav-Gal4*; central neurons, *elav-Gal4*; motor neurons, *ok371-Gal4*; central glia, *repo-Gal4*) were dissected to isolate the tissue of interest. Bodywalls or brains were dissociated and Red-Stinger-labeled cells were isolated by flow cytometry into RNAqueous lysis buffer. Samples were sequenced as 51 base single end reads on a HiSeq 2500 running in high-output mode at the UCSF Center for Advanced Technology, with read depths ranging from 1.5 to 18.4 million reads. Reads were demultiplexed with CASAVA (Illumina) and read quality was assessed with FastQC (http://www.bioinformatics.babraham.ac.uk/projects/fastqc/). Reads were aligned to the *D. melanogaster* transcriptome, FlyBase genome release 6.10, using STAR version 2.5.2b (Dobin et al., 2013) with the option '–quantMode TranscriptomeSAM'. Transcript expression was modeled from these STAR alignments using Salmon (Patro et al., 2017) in alignment-based mode. The raw sequencing reads and gene expression estimates are available in the NCBI Sequence Read Archive (SRA) and in the Gene Expression Omnibus (GEO) under accession number GSE120305. The da neuron and whole larvae datasets were previously described and published and are available from SRA and GEO under accession numbers GSE72884 and GSE99711, respectively.

Plasmid Constructs

Expression constructs for dTAT were generated using PCR from a synthetic template (dTATalt) in which the wobble position of each codon was conservatively replaced, making them refractory to RNAi (Blue Heron Biotech). The GFP-dTATalt fusions were cloned by 5′ overlapping extension PCR using primers listed in Table S3. GFP-dTATalt inserts were cloned into the KpnI/ApaI sites of pMT B V5/His (Invitrogen) for copper-inducible expression in S2 cells or into the EcoRI/NotI sites in pBID-UASC (Addgene) for generating transgenic fly lines. The catalytically inactive version of dTAT was generated by mutating two glycine residues (G133 and G135) to tryptophan to disrupt acetyl CoA binding (Topalidou et al., 2012).

Identification of candidate *Drosophila* acetylases

Drosophila homologs of GCN5, ELP3, ARD1, and NAT1 have been studied in other contexts, but their roles in microtubule acetylation have not been characterized. We additionally identified the GNAT domain-containing lethal(1)G0020/CG1994 as the likely NAT10 homolog (53.8% identity) and CG3967 and CG17003 as potential αTAT/MEC-17 homologs (CG3967, 38.8% identity; CG17003, 34.7% identity)

S2 cell culture, RNAi, and immunofluorescence

Culture and RNAi of *Drosophila* S2 cells were performed as previously described (Rogers and Rogers, 2008). S2 cells (*Drosophila* Genomics Resource Center, Bloomington, IN) were cultured in SF900II medium supplemented with 100x antibiotic-antimycotic (Invitrogen, Carlsbad, CA). DNA templates for dsRNA synthesis were obtained by PCR amplification of the pFastBacHT-CAT expression plasmid (Invitrogen), BDGP cDNA clones, or S2 cell genomic DNA using the gene-specific primer sequences (Table S4). As a negative control, a sequence from chloramphenicol acetyltransferase (CAT) was amplified and transcribed into dsRNA. *In vitro* transcription reactions were performed with T7 RNA polymerase purified in house. Cells were transfected using Fugene HD (Promega) according to the manufacturer's instructions. Stable cell lines were selected by supplementing culture medium with 10 μg/mL blasticidin or 500 ug/mL hygromycin (Invitrogen). Immunofluorescence was performed by plating cells into fabricated 35 mm glass bottom culture dishes pre-coated with concanavalin A in serum-free Schneider's medium (Sigma). After cells had attached and spread for 1 hour, they were fixed with 10% formaldehyde (EM Sciences) in HL3 buffer (70 mM sodium chloride; 5 mM potassium chloride; 20 mM magnesium chloride hexahydrate; 10 mM sodium bicarbonate; 5 mM trehalose; 115 mM sucrose; 5 mM HEPES; pH 7.2) for 10 minutes. Cells were permeabilized and blocked with 5% bovine serum albumin in TBST (TBS + 0.1% Triton X-100) before staining with primary and secondary antibodies. Cells were imaged on an Eclipse Ti-E microscope with a 100x oil NA-1.45 objective, driven by NIS Elements software. Images were captured with a cooled charge-coupled device camera (CoolSNAP HQ, Roper Scientific).

Antibodies

The following antibodies were used in this study: anti-acTb (6-B11-1, Sigma), anti-α-tubulin (DM1α, Sigma), FITC-labeled DM1α monoclonal antibodies (Sigma), anti-GFP (A-11122, Fisher), anti-DsRed (632496, Clontech), Anti-Myc (9E11, DSHB), Anti-Futsch (22C10, DSHB), Cy5-conjugated anti-HRP (Jackson immunoresearch), and Alexa Fluor conjugated secondary antibodies (Fisher). In order to generate antibodies against dTAT, we used PCR to amplify the catalytic domain (residues 1 to 196) and cloned this fragment into the NheI/ XbaI sites of pET28a or the BamHI/NotI sites of pGEX6P2. Recombinant dTAT 1-196 was expressed in *E. coli* and purifiied on NiNTA resin (QIAGEN) and glutathione-Sepharose, respectively. Purified 6xhis-dTAT1-196 protein was used to generate polyclonal antibodies in rabbits (Pocono Rabbit Farm) and the antibodies were further affinity-purified on GST-dTAT 1-196 bound to amino-link resin (Thermo Fisher Scientific). Secondary antibodies for immunofluorescence were purchased from Jackson Immunoresearch. HRP-conjugated secondary antibodies for immunoblots were purchased from Sigma.

Imaging of larval samples

Live imaging

Larvae were mounted in 90% glycerol under No. 1 coverslips and imaged using a Leica SP5 microscope with a 40 × 1.2 NA lens. For time-lapse analysis, larvae were imaged at the indicated time, recovered to yeasted agar plates with vented lids, aged at 25°C, and imaged again.

EB1 assays

Larvae were carefully mounted and imaged, then immediately placed in a small plastic Petri dish and stimulated with forceps pinches to segments A2, A3, and A4 and re-imaged under the same conditions. Maximum projections of confocal z stacks (1 μm z step size) were set to identical threshold levels to eliminate non-punctate signals and quantified in Fiji (Schindelin et al., 2012).

Immunostaining

Larval immunostaining was performed as described (Jiang et al., 2018) with the exception of fixation in freezing methanol for 15 min for AcTb staining. Antibody dilutions were as follows: acTb, 1:1000; GFP, 1:100; 22c10 (1:200); HRP-Cy5 (1:100), secondary antibodies (1:200).

Expansion microscopy

Following immunostaining with Mouse anti-GFP, clone 3E6 (Invitrogen #A11120, 1:100) and Goat anti-Mouse Alexa488 (Thermofisher A31561, 1:100) as previously described (Jiang et al., 2018), samples were mounted on lysine-coated #1.5 cover glass in polydimethylsiloxane wells and incubated in monomer solution (2 M NaCl, 8.625% Sodium Acrylate, 2.5% Acrylamide, 0.15% Bisacrylamide in PBS) for 1 h at 4°C prior to gelation. A stock of 4-hydroxy-2,2,6,6-tetramenthylpiperidin-1-oxyl (4-hydroxy-TEMPO) at 1% (wt/wt) in water was added to the incubation solution and diluted to concentration of 0.01%. Concentrated stocks of tetramethylethylenediamine (TEMED) and ammonium persulfate (APS) at 10% (wt/wt) in water were added sequentially to the incubation solution and diluted to concentrations of 0.2% (wt/wt). The tissues were then incubated at 37°C for 3-4 h. After gelation, the gels were cut and placed in a small 12-well chamber and 1mg/ml of Chitinase in PBS (pH 6.0) was used to digest the cuticles for ~4 d at 37°C. Chitinase-treated samples were incubated with 1000 units/ml collagenase solution (prepared with buffer 1x HBSS lacking calcium, magnesium, and phenol red) with 0.01 M $CaCl_2$ and 0.01 M $MgCl_2$ overnight in a 37°C shaking incubation chamber. Samples were then rinsed with PBS twice for 5 min and digested in 8 units/ml proteinase K solution in digestion buffer (40 mM Tris pH 8.0, 1 mM EDTA, 0.5% Triton, 0.8 M Guanidine HCl) for 1 h at 37°C. Subsequently, samples were removed from the digestion solution and were allowed to expand in excess water overnight. After expansion, the expanded gel was trimmed to fit onto the coverglass, excess water was removed, and the gel was mounted on a lysine-coated cover glass for imaging. Confocal microscopy was performed on a Leica SP5 inverted confocal scanning microscope using a 63 × 1.2 NA water lens.

Calcium imaging

Third-instar larvae were dissected in calcium imaging solution (310mOsm, pH7.2) containing (in mM): NaCl 120, $MgCl_2$ 4, KCl 3, $NaHCO_3$ 10, Glucose 10, Sucrose 10, Threalose 10, TES 5, HEPES 10. Larvae were pinned ventral side up on Sylgard® 184 silicone elastomer plates. After opening the larval body from the ventral side, internal organs were removed, and the muscle covering the dorsal c3 da neuron (ddaF) was also gently removed to facilitate imaging of ddaF in segments A4 to A6.

Stimulation electrodes (sealed/polished with a diameter of ~10 μm) were mounted in contact with the internal side of the larval body wall within the dendritic filed of the target c3 da neuron. The tip position was set to avoid direct contact with dendritic tips for potential damage. Following 20ms transient vertical stimulations, each with increasing displacements (10, 20, 30, 40, 50 and 60 μm; applied with a Sutter MP-285 micromanipulator), the electrode was returned to the starting position. GCaMP6s fluorescence was excited with a 488nm solid-state laser and GCaMP fluorescence was imaged at a 0.97Hz frame acquisition rate using a W Plan-APOCHROMAT 20 × /1.0 objective lens and a Zeiss LSM 700 confocal microscope. Changes in calcium levels in the cell body were measured using the following formula:

$$\Delta F/F_0 = (F_{peak}\text{-}F_0)/F_0$$

where $\mathbf{F_0}$ is the average fluorescence in 30 s right before vertical mechanical stimulation. $\mathbf{F_{peak}}$ is defined as the maximum fluorescence upon stimulation.

Behavior assays

Gentle touch

Each larva was stimulated with an eyelash stroke on thoracic segments while in a bout of linear locomotion. The stimulus was applied and scored four times per larva, with responses scored as previously described (Kernan et.al 1994). Tests were performed with the experimenter blind to genotype in this and all other behavior assays.

Harsh Touch

Larvae were placed in a plastic Petri dish with enough water, so larvae remained moist, but not floating in the dish. Von frey filaments made from fishing line and affixed to glass capillaries were applied to the dorsal side of the larvae between segments A3-A6 until the filament buckled, exhibiting a pre-determined force. Forces of 44mN, 78mN and 98mN were used in this study. A positive response was scored if one complete nocifensive roll occurred after the first mechanical stimulus.

Sound/vibration

Wandering third instar larvae were picked from a vial and washed with PBS. 10 larvae were placed on a 1% agar plate on top of a speaker and stimulated as previously described (Zhang et al., 2013). A 1 s 70dB, 500Hz pure tone was played 10 times with 4 s of silence in between. Video recordings captured larval behavior, with the number of times out of 10 each larva exhibited sound startle behavior as its individual score. 3 separate trials were performed for each genotype. Videos were recorded with AmScope MU300 Microscope digital camera. Larval startle behavior was scored as responsive with the following behaviors: mouth-hook retraction, pausing, excessive turning, and/or backward locomotion.

Gravitaxis

A RING apparatus was assembled as described (Kamikouchi et al., 2009) using 2.3 cm diameter, 9.5 cm polypropylene *Drosophila* vials. 25 flies were collected, aged until all the flies were 5-8 days old, and transferred to a gravitaxis vial sealed with parafilm. The apparatus was rapped on a table five times in rapid succession to initiate the gravitaxis response. Videos of the flies were captured and position of each fly in the tube was determined 4 s after the response initiation. Flies were allowed to rest 1 minute, and this was repeated for 5 total trials, for n = 1. Assays were repeated for each genotype for total n = 3

Thermal Nociception

Local heat probe assays were performed as previously described (Chattopadhyay et al., 2012). Washed larvae were placed on a piece of vinyl and stimulated on their dorsal midline at segment A4 with a thermal probe maintained at 38c°C for a maximum of 20 s or until completion of a rolling nocifensive response.

Larval locomotion

Larvae were washed and placed on an agar plate with a paint brush, allowed to habituate for 1 minute, and subsequently 10 s videos of individual crawling larvae were recorded in LAS as uncompressed avi files. Files were converted to flymovieformat with any2ufmf and analyzed in Ctrax (Branson et al., 2009). Videos were recorded on Leica DFC310 FX camera on an AmScope FMA050 mount.

Taxol Feeding

Third instar larvae were transferred to 35 mM dishes of cornmeal-molasses food containing DMSO (vehicle) or 60uM taxol (unless otherwise indicated) for 3 hours and then subject to behavior analysis. Adult flies were starved overnight (16 hours) and then fed a 5% sucrose solution containing DMSO or 60uM taxol for 5 hours prior to behavioral analysis.

Electrophysiology

We adapted the methods of (Gong et al., 2013) to record NOMPC-mediated mechanically evoked responses from central neurons in the *Drosophila* ventral nerve cord (VNC). Adult physiology preparations were as previously described with some modification (Tuthill and Wilson, 2016). Flies were cold-anesthetized and fixed with their ventral side facing up to the underside of a custom-milled steel platform using UV-cured glue (KOA 300, KEMXERT). The ventral head and anterior thorax were partly inserted through a hole in the platform. The top side of the platform, and thus also the exposed parts of the head and thorax, were continually perfused with oxygenated saline. All six legs were glued to the holder with UV-cured glue. A small hole was manually dissected in the cuticle of the ventral thorax to expose the prothoracic neuromeres, and the perineural sheath was gently removed with fine forceps to expose neuronal cell bodies.

The preparation was perfused at ~2-3 ml/min with saline (103 mM NaCl, 3 mM KCl, 5 mM TES, 8 mM trehalose, 10 mM glucose, 26 mM $NaHCO_3$, 1 mM NaH_2PO_4, 1.5 mM $CaCl_2$, and 4 mM $MgCl_2$; pH 7.1, osmolality adjusted to 270-275 mOsm) bubbled with 95% O2/5% CO_2. Recordings were performed at room temperature. Cell bodies were visualized using an infrared LED (Smartvision) and a 40 × water-immersion objective on an upright compound microscope equipped with a fluorescence attachment (Sutter SOM). Whole-cell patch-clamp recordings were targeted to GFP-labeled cell bodies in the prothoracic region of the VNC. The internal patch pipette solution contained (in mM): 140 potassium aspartate, 10 HEPES, 1 EGTA, 4 MgATP, 0.5 Na_3GTP, 1 KCl, and 13 biocytin hydrazide (pH 7.2, osmolarity adjusted to ~265 mOsm). We distinguished MNs from other glutamatergic neurons by the characteristic and reliable positions of their cell bodies (Baek and Mann, 2009; Brierley et al., 2012), as well as their intrinsic properties (input resistance, resting membrane potential, and spike waveform).

All recordings were made in current-clamp mode using an Axopatch 700A amplifier. Data were low-pass filtered at 5 kHz before they were digitized at 10 kHz by a 16 bit A/D converter (National Instruments, USB-6343), and acquired in MATLAB. Stable recordings were typically maintained for ~1 hour. A small hyperpolarizing current (approximately −5 to −10 pA) was injected to compensate for the depolarizing seal conductance (Gouwens and Wilson, 2009). Analysis of electrophysiology data was performed with custom scripts written in MATLAB and Python.

Motor neurons were mechanically stimulated with a closed-loop piezoelectric actuator (Physik Instrumente P-841.60, 90 μm travel range, with E-509.S1 sensor/piezo servo-control module). Mechanical stimuli were generated in MATLAB and sent to the amplifier at 5 kHz using an analog output DAQ (National Instruments 9263). Mechanical stimuli were generated in MATLAB and sent to the amplifier at 5 kHz using an analog output DAQ (National Instruments 9263). The stimulating pipette was positioned next to the ipsilateral VNC neuromere under visual control. A 12 μm square wave was used to indent the neuropil. Because the MN cell bodies are segregated from the VNC neuropil, the mechanical stimuli had no visible effect on the cell body and patch pipette. Stimulation of the contralateral neuromere failed to evoke a response.

Atomic force microscope measurements

The elastic moduli of control- and *dTat* RNAi-treated cells were measured using an MFP-3D Bio AFM (Asylum Research, Santa Barbra, CA). The AFM head was mounted on an Olympus IX71 inverted optical microscope to aid in accurately positioning the cantilever probe directly above a single cell. Cells were probed using a Novascan silicon nitride AFM cantilever of nominal spring constant 0.03N/m with a 4.5um polystyrene bead attached. Before force measurements were made on each sample, the cantilever spring constant was calibrated using the built-in thermal tune method in the IGOR/Asylum Software. These calibrations ranged from 0.039-0.042N/m.

S2 cell RNAi was performed for seven days as described above; we then treated with dsRNA every other day to maintain protein depletion. On the day of an experiment, confluent cells from each population (control or *dTat* RNAi) were plated on cleaned glass poly L-lysine-coated coverslips such that adherent cells were spaced about 2-3 cell diameters apart once attached. Stiffness measurements were acquired 45 min to 120 min after plating at room temperature. Parallel samples of control or *dTat* RNAi cells were plated and an approximately equivalent number of data points were acquired during each trial. The order of data acquisition was varied for each experiment.

For force versus indentation measurements the cantilever was moved at a velocity of 5 μm/s toward the cell until a force of 3 nN was reached. The cantilever was then retracted at the same rate. For most cells, this was equivalent to an indentation of 3-4 μm. For each cell, two force curves were collected and one was chosen, based on clearly defined points of contact and flat baseline approaches. The first curve was picked in approximately 80% of all cells. Force measurements were acquired for ~300 cells of each type over a period of three days of experiments.

Calibrated cantilever deflection and piezo displacement data collected were converted to produce force versus indentation curves (Figure S7). Using a custom MATLAB code, force-indentation data were fit to the Hertzian contact mechanics model to determine elastic moduli (stiffness) for each cell (Beicker et al., 2018; Cribb et al., 2016). The force versus indentation data were fit up to indentations of 750nm which corresponded to less than 10% of the cell height. The entire dataset was screened for relative RMS fitting errors greater than two sigma above the mean. Then, elastic moduli values that were above or below two sigma of the mean were excluded within each trial (Grubbs, 1950).

QUANTIFICATION AND STATISTICAL ANALYSIS

Datasets were tested for normality using Shapiro-Wilks goodness of fit tests. Details on statistical tests are provided in figure legends and the corresponding methods sections.

DATA AND SOFTWARE AVAILABILITY

D. melanogaster larval cell type RNA-Seq data are available from SRA and GEO under the accession number GEO: GSE120305.

Cell Reports, Volume *25*

Supplemental Information

Microtubule Acetylation Is Required for Mechanosensation in *Drosophila*

Connie Yan, Fei Wang, Yun Peng, Claire R. Williams, Brian Jenkins, Jill Wildonger, Hyeon-Jin Kim, Jonathan B. Perr, Joshua C. Vaughan, Megan E. Kern, Michael R. Falvo, E. Timothy O'Brien III, Richard Superfine, John C. Tuthill, Yang Xiang, Stephen L. Rogers, and Jay Z. Parrish

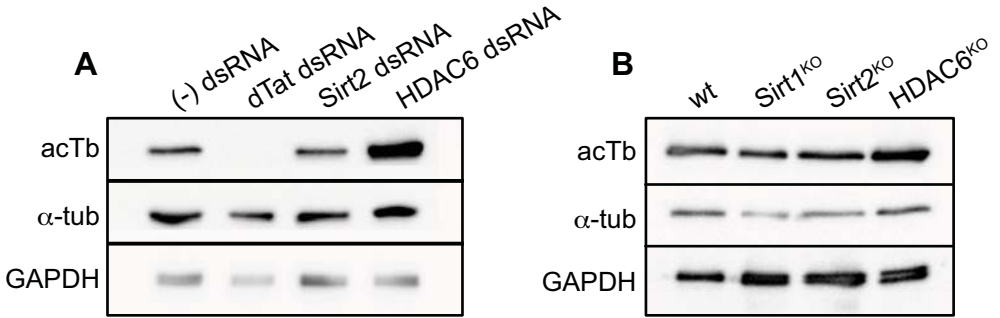

Figure S1. Related to Figure 1. HDAC6 is the major alpha tubulin deacetylase in *Drosophila*. (A) Western blots of cell lysates from S2 cells treated with dsRNA to the indicated genes showing that *HDAC6* RNAi leads to increased levels of acTb. (B) Western blots of larval lysates from the indicated genotypes showing that loss of *HDAC6* function leads to increased accumulation of acTb *in vivo*.

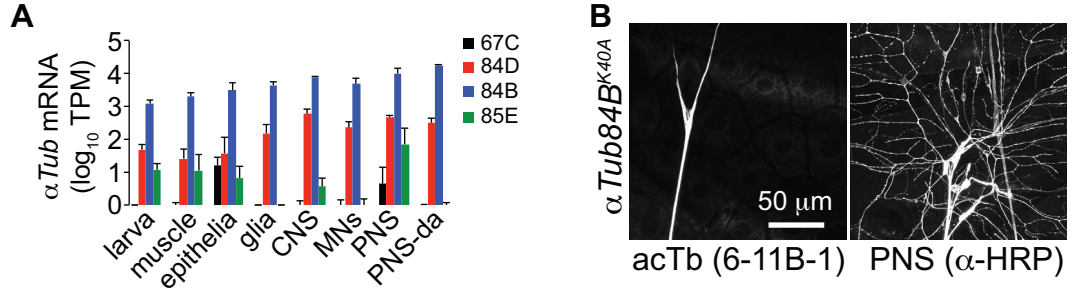

Figure S2. Related to Figure 3. αTubulin K40 is required for tubulin acetylation. (A) Larval mRNA expression of the *Drosophila αTubulin* isotypes in the indicated cell types; *αTub84B* accounts for >90% of *α Tubulin* mRNA in the PNS. (B) acTb staining in *αTub84B*^{K40A} mutant third instar larva showing that the *αTub84B* isotype accounts for the majority of acTb in larvae.

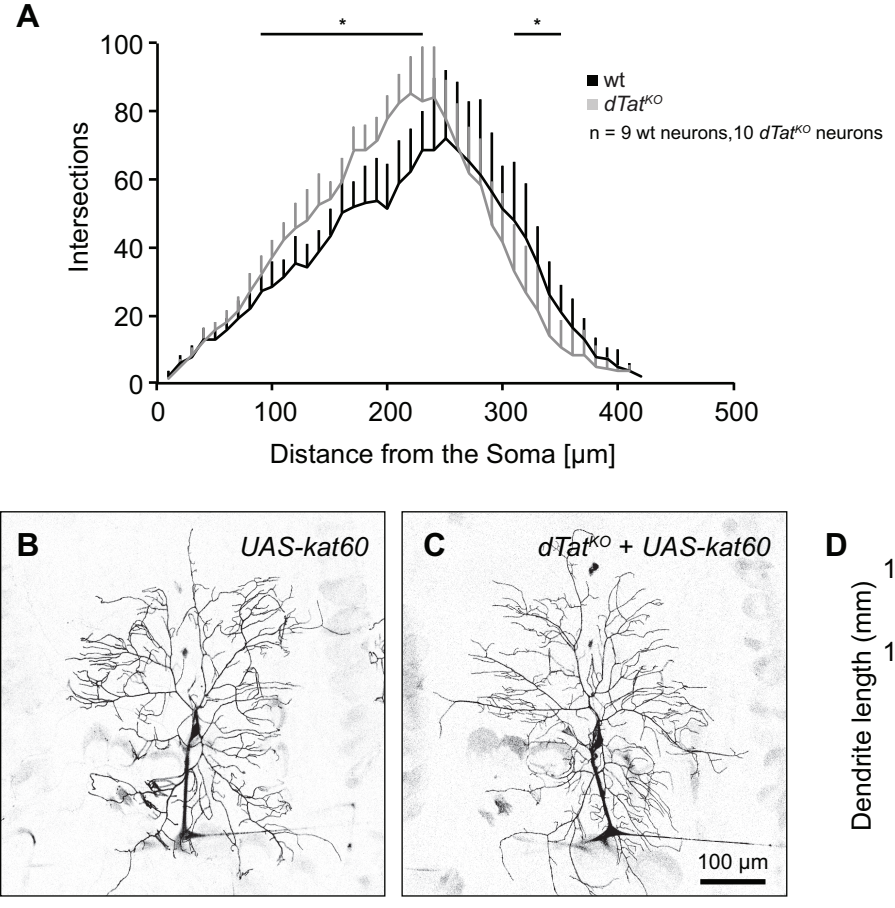

Figure S3. Related to Figure 4. (A) *dTat* has a minor effect on dendrite branch distribution. Sholl analysis depicting mean number and standard deviation of dendrite intersections as a function of distance from soma for 9 wt C4da neurons and 10 *dTat*^{KO} mutant C4da neurons. *P < 0.05 compared to wt controls, Welch's t-test. (B-D) *dTat* has no effect on *katanin*-induced remodeling of c4da dendrite arbors. Representative images of control larvae (B) or *dTat*^{KO} mutant larvae (C) overexpressing *katanin* (*UAS-kat60*) in c4da neurons under the control of *ppk-Gal4*. Dendrites were labeled with the c4da-specific marker *ppk-CD4-tdTomato* visualized via live confocal imaging. (D) Quantification of total dendrite length for the indicated genotypes. Boxes mark 1st and 3rd quartiles, bands mark medians, whiskers mark 1.5 x IQR, and outliers are shown as points. Welch's test of unequal variance revealed no significant difference was detected between the two groups.

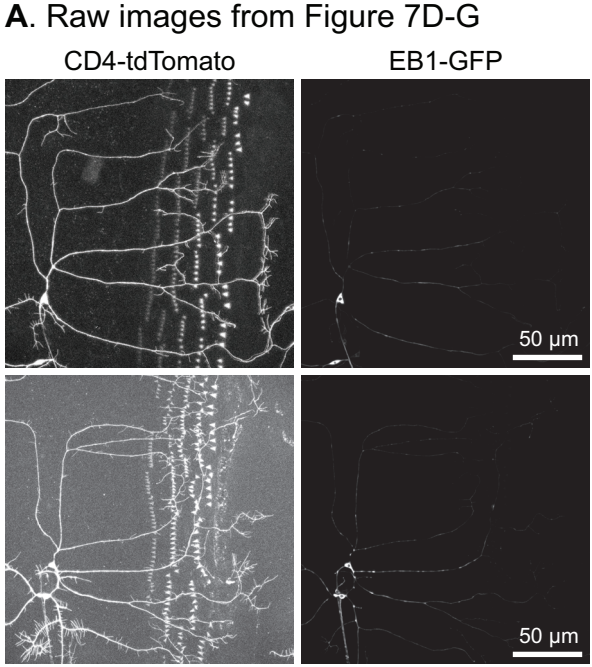

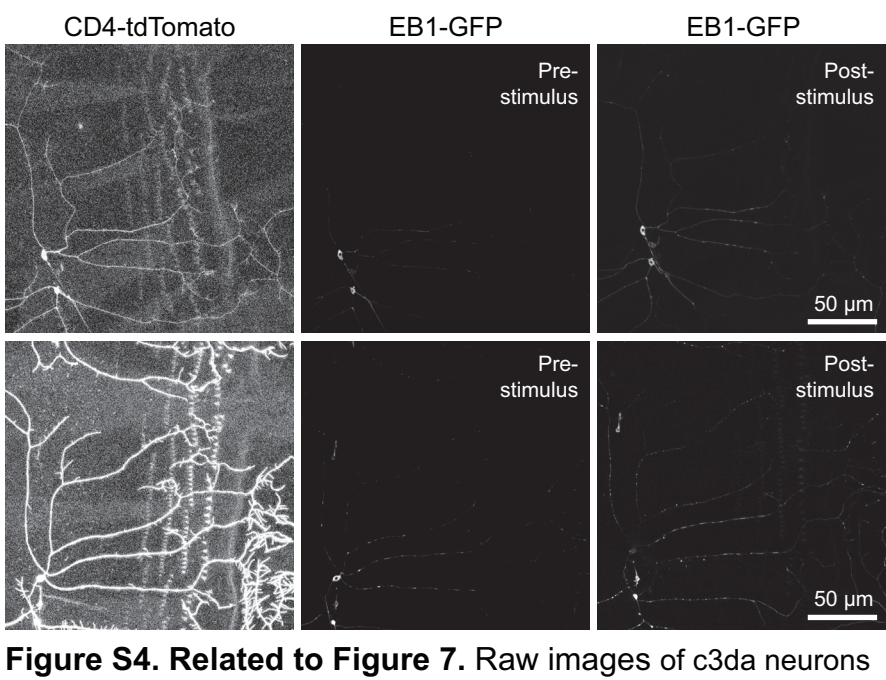

Figure S4. Related to Figure 7. Raw images of c3da neurons expressing EB1-GFP to label microtubule plus ends and the membrane marker CD4-tdTomato from (A) untreated wild type or *dTat*^{KO} mutant larvae and (B) wild type and *dTat*^{KO} mutant larvae that were subjected to mechanical stimulus.

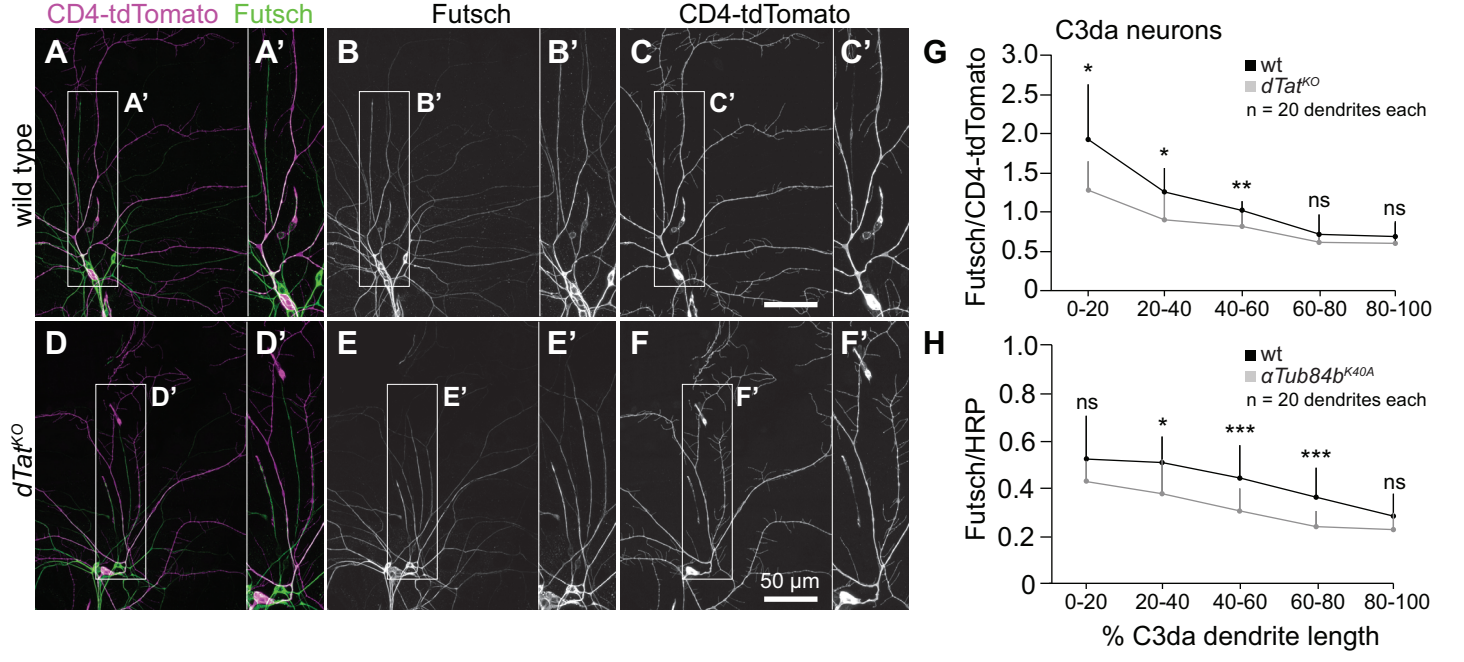

Figure S5. Related to Figure 7. Loss of acTb alters composition of the microtubule cytoskeleton in c3da neurons. Representative images of da neuron arbors immunostained for CD4-tdTomato (A, D), Futsch (B, E), or both (C, F) are shown for wild type (A-C) and *dTat*^{KO} mutant (D-F) third instar larvae expressing the membrane marker CD4-tdTomato in c3da neurons (*nompC-Gal4, UAS-CD4tdTomato*). (G) Quantification of Futsch intensity (means ± s.d.) in c3da neurons is shown for wild type and *dTat*^{KO} mutants. Futsch levels were measured along c3da dendrites (0-100% dendrite length, originating at the soma) and normalized to CD4-tomato levels. (H) Quantification of Futsch intensity (means ± s.d.) in c3da neurons is shown for wild type and *αTub84B*^{K40A} mutants with Futsch intensity normalized to HRP levels. ns, not significant, *P<0.05, ***P<0.001 compared to wt controls, unpaired t-test with Welch's correction.

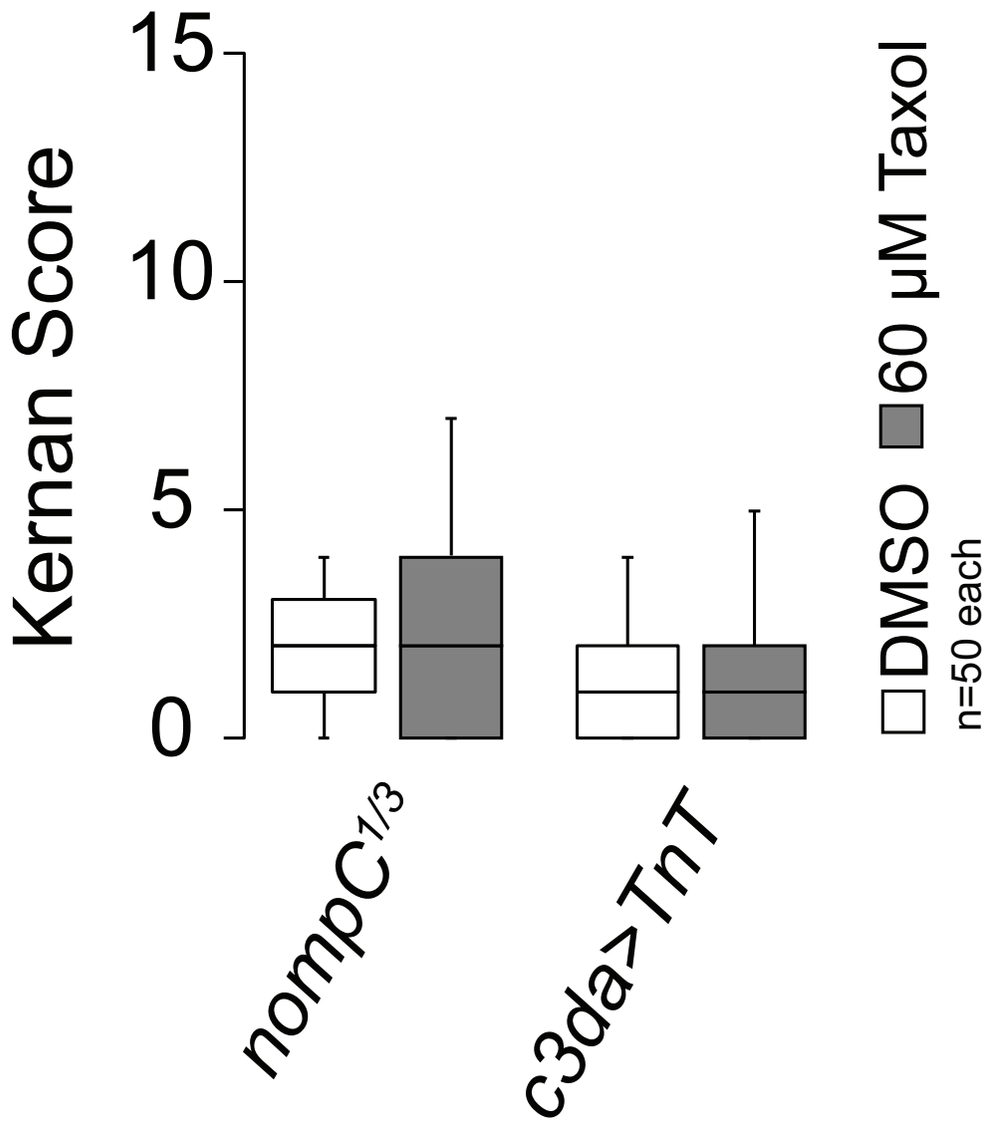

Figure S6. Related to Figure 7. Taxol enhancement of gentle touch responses depends on activity of NOMPC and c3da neurons. Boxplots depict behavioral responses of third instar larvae of the indicated gentoypes to gentle touch stimulus at 96 h after egg laying (AEL). Mutation of *nompC* or blocking synaptic transmission by expressing Tetanus toxin in c3da neurons (*c3da>TnT*) rendered taxol-fed larvae insensitive to gentle touch.

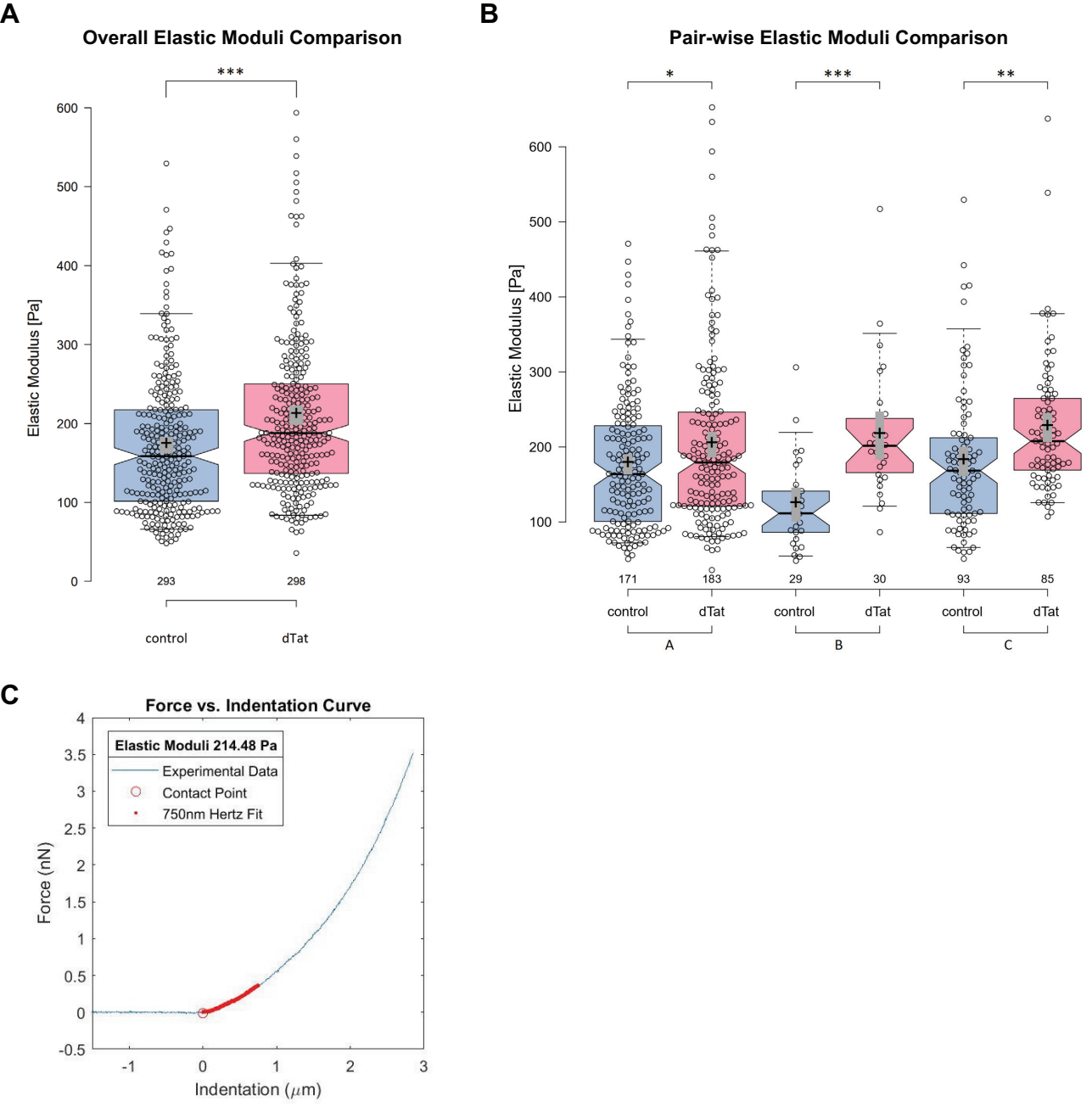

Figure S7. Related to Figure 7. dTAT regulates cellular rigidity in S2 cells. (A) Plots show the pattern of stiffness data for a combined 3 days of experiments, with the median (central bar) and mean (+ sign) shown. Means of 172 Pa for control and 211 Pa for *dTat* RNAi are significantly different to p < 0.0001. The medians of each were control: 158.5 Pa; *dTat* RNAi: 187.9 Pa, and the Mann Whitney comparison was also significant > 0.0001. (B) The paired comparisons of the cellular stiffness data shown in (A). The waist of the boxplots indicates the median and the height of the notches represents the 95% confidence interval of the median. The mean is denoted by the plus sign and the grey box represents the 95% confidence interval of the mean. The whiskers extend from the 5th to the 95th percentile. Statistical significance is marked as follows: "***" for a p-value < 0.001, "**" for a p-value between 0.001 and 0.005, and "*" for a p-value < 0.05. Significance levels for each pair, based on the student's t-test, assuming unequal variance, are indicated in Table S2. Each pair was derived from cells separately grown and maintained; no wells were re-used. (C) Characteristic Force vs. Indentation curve fit to the Hertz model. The plot shows the entire force-indentation curve in blue, a red circle for the contact point, and the Hertz model fit for 750 nm indent in red. Within the Hertz model, force increases as the 3/2 power of indentation. Here this fitting resulted in a cell modulus of 214 Pa.

Table S1. Related to Figure 5. Expression levels of mechanosensory channels in different cell types.

	PNS	da neurons	motoneurons
CG46121	56.91	7.10	0
iav	3.26	0	4.59
nan	0	0.02	0.19
nompC	87.84	22.92	0
pain	6.23	4.08	0.51
Piezo	16.93	100.48	4.00
ppk	272.00	398.80	0
ppk26	628.29	650.44	0
rpk	0	0	0
trp	0	0	0
Trpgamma	0	0	0.02
trpl	20.83	0.03	0
wtrw	0.25	0	0

Mean mRNA expression levels (tpm, transcripts per million) are shown for mechanosensory channel genes in each of the indicated cell types. N = 4 independent samples for PNS and da neurons; 7 independent samples for motoneurons.

Table S2. Related to STAR Methods. Means, medians and significance values for AFM measurements.

	Pair A		Pair B		Pair C	
Mean [Pa]	176.8	203.0	123.2	215.3	180.7	226.1
Median [Pa]	163.8	179.3	111.5	201.6	168.4	207.7
p (same mean)	0.016		1.08E-05		9.88E-04	
	*		***		**	

Significance levels for each pair were calculated with the Student's t-test assuming unequal variance. Statistical significance is marked as follows: "***" for a p-value < 0.001, "**" for a p-value between 0.001 and 0.005, and "*" for a p-value < 0.05.

Table S3. Related to Figures 1-7. Experimental genotypes used in this study.	
Figure 1E	
wt	w^{1118}
$dTat^{KO}$	w^{1118}; +; $dTat^{KO}$ / $dTat^{KO}$
Figure 2A	
Larva	w^{1118}
Muscle	w^{1118}; *MHC-Gal4* / *UAS-nls-GFP*
Epi.	w^{1118}; *UAS-nls-GFP* / + ; *A58-Gal4* / +
Glia	w^{1118}; *UAS-nls-GFP* / + ; *repo-Gal4* / +
CNS	w^{1118}, *elav-Gal4* / + ; *UAS-nls-GFP* / +
MNs	w^{1118}; *UAS-nls-GFP* / + ; *Vglut-Gal4* / +
PNS	w^{1118}, *elav-Gal4* / + ; *UAS-nls-GFP* / +
PNS-da	w^{1118}; *21-7-Gal4* / *UAS-nls-GFP*
Figure 2B-2C	
wild type	w^{1118}
Figure 2D-2G	
$dTat^{GFP}$	w^{1118}; +; $dTat^{GFP}$ / $dTat^{GFP}$
Figure 2H-2K	
wild type	w^{1118}
$dTat^{KO}$	w^{1118}; +; $dTat^{KO}$ / $dTat^{KO}$
Figure 2L-2O	
$dTat^{KO}$ + *19-12>GFP-dTat*	w^{1118}; *UAS-GFP-dTat-L* / +; *19-12-Gal4*, $dTat^{KO}$ / $dTat^{KO}$
Figure 3A	
wt	w^{1118}
$dTat^{KO}$	w^{1118}; +; $dTat^{KO}$ / $dTat^{KO}$
$dTat^{KO / Df}$	w^{1118}; +; $dTat^{KO}$ / *Df(3L)BSC113*
$\alpha Tub84B^{K40A}$	w^{1118}; +; $\alpha Tub84B^{K40A}$ / $\alpha Tub84B^{KO}$
$\alpha Tub84B^{K40R}$	w^{1118}; +; $\alpha Tub84B^{K40R}$ / $\alpha Tub84B^{KO}$
$dTat^{KO}$, $\alpha Tub84B^{K40A}$	w^{1118}; +; $dTat^{KO}$, $\alpha Tub84B^{K40A}$ / $dTat^{KO}$, $\alpha Tub84B^{K40A}$
Figure 3B	
c3da-Gal4 / +	w^{1118}; *nompC-Gal4* / +
UAS-dTat / +	w^{1118}; *UAS-GFP-dTat-L* / +
$dTat^{KO}$ + *c3da>dTat*	w^{1118}; *nompC-Gal4* / *UAS-GFP-dTat-L*; $dTat^{KO}$ / $dTat^{KO}$
c3da>dTat	w^{1118}; *nompC-Gal4* / *UAS-GFP-dTat-L*
$HDAC6^{KO}$	y^{1}, w^{1118}, $HDAC6^{KO}$
$\alpha Tub84B^{K40R}$ + *c3da>dTat*	w^{1118}; *nompC-Gal4* / *UAS-GFP-dTat-L*; $\alpha Tub84B^{K40R}$ / $\alpha Tub84B^{K40R}$
Figure 3C	
wt	w^{1118}
$dTat^{KO}$	w^{1118}; +; $dTat^{KO}$ / $dTat^{KO}$
Figure 3D	
wt	w^{1118}
c4da>Kir	w^{1118}; +; *ppk-Gal4* / *UAS-KIR2.1*
$dTat^{KO}$	w^{1118}; +; $dTat^{KO}$ / $dTat^{KO}$

αTub84B^{K40A}	*w^{1118}; +; αTub84B^{K40A} / αTub84B^{KO}*
dTat^{KO} + c4da>dTat	*w^{1118}; UAS-GFP-dTat-L / +; ppk-Gal4, dTat^{KO} / dTat^{KO}*
Figure 3E-3F	
wt	*w^{1118}*
dTat^{KO}	*w^{1118}; +; dTat^{KO} / dTat^{KO}*
αTub84B^{K40A}	*w^{1118}; +; αTub84B^{K40A} / αTub84B^{KO}*
dTat^{KO} + cho>dTat	*w^{1118}; UAS-GFP-dTat-L / nompC-Gal4; dTat^{KO} / dTat^{KO}*
Figure 3G	
wt	*w^{1118}*
c4da>Kir	*w^{1118}; +; ppk-Gal4 / UAS-KIR2.1*
dTat^{KO}	*w^{1118}; +; dTat^{KO} / dTat^{KO}*
αTub84B^{K40A}	*w^{1118}; +; αTub84B^{K40A} / αTub84B^{KO}*
Figure 3H	
wt	*w^{1118}*
dTat^{KO}	*w^{1118}; +; dTat^{KO} / dTat^{KO}*
αTub84B^{K40A}	*w^{1118}; +; αTub84B^{K40A} / αTub84B^{KO}*
Figure 4A-4D	
wild type	*w^{1118}; nompC-Gal4, UAS-CD4-tdGFP / +*
dTat^{KO}	*w^{1118}; nompC-Gal4, UAS-CD4-tdGFP / +; dTat^{KO} / dTat^{KO}*
Figure 4E-4G	
wt	*w^{1118}*
dTat^{KO}	*w^{1118}; +; dTat^{KO} / dTat^{KO}*
Figure 4H-4L	
wild type	*w^{1118}, ppk-mCD8-GFP*
dTat^{KO}	*w^{1118}, ppk-mCD8-GFP; +; dTat^{KO} / dTat^{KO}*
Figure 5A-5C	
wt	*w^{1118}; nompC-Gal4 / UAS-GCaMP6s*
dTat^{KO}	*w^{1118}; nompC-Gal4 / UAS-GCaMP6s; dTat^{KO} / dTat^{KO}*
αTub84B^{K40A}	*w^{1118}; nompC-Gal4 / UAS-GCaMP6s; αTub84B^{K40A} / αTub84B^{K40A}*
Figure 5D	
dTat^{KO}	*w^{1118}; +; dTat^{KO} / dTat^{KO}*
nompC$^{1/3}$	*w^{1118}; nompC^{1}/ nompC^{3}*
c3da>TnT	*w^{1118}; nompC-Gal4 / UAS-Tetanus Toxin*
nompC$^{1/3}$; dTat^{KO}	*w^{1118}; nompC^{1}/ nompC^{3}; dTat^{KO} / dTat^{KO}*
Figure 5F-5G	
Vglut>GFP	*w^{1118}; OK377-Gal4, UAS-mCD8-GFP / +*
Vglut>nompC	*w^{1118}, UAS-GFP-nompC; OK377-Gal4, UAS-mCD8-GFP / +*
Vglut>nompC; dTat^{KO}	*w^{1118}, UAS-GFP-nompC; OK377-Gal4, UAS-mCD8-GFP / +; dTat^{KO} / dTat^{KO}*
Figure 6A	
wild type	*w^{1118}, UAS-GFP-nompC; nompC-Gal4, UAS-mCD4-tdTomato / +*
dTat^{KO}	*w^{1118}, UAS-GFP-nompC; nompC-Gal4, UAS-mCD4-tdTomato / +; dTat^{KO} / dTat^{KO}*
Figure 7A-7H	

wild type	w^{1118}; *nompC-Gal4, UAS-mCD4-tdTomato / UAS-EB1-GFP*
$dTat^{KO}$	w^{1118}; *nompC-Gal4, UAS-mCD4-tdTomato / UAS-EB1-GFP*; $dTat^{KO}$ / $dTat^{KO}$
Figure 7I	
wild type	w^{1118}
Figure 7J-7M	
wt	w^{1118}
$dTat^{KO}$	w^{1118}; +; $dTat^{KO}$ / $dTat^{KO}$
$\alpha Tub84B^{K40A}$	w^{1118}; +; $\alpha Tub84B^{K40A}$ / $\alpha Tub84B^{KO}$
Supplemental Figure S1B	
wt	w^{1118}
$Sirt1^{KO}$	w^{1118}; $Sirt1^{2A-7-11}$
$Sirt2^{KO}$	w^{1118}; $Sirt2^{5B-2-35}$
$HDAC6^{KO}$	y^{1}, w^{1118}, $HDAC6^{KO}$
Supplemental Figure S2a	
Larva	w^{1118}
Muscle	w^{1118}; *MHC-Gal4* / *UAS-nls-GFP*
Epi.	w^{1118}; *UAS-nls-GFP / + ; A58-Gal4 / +*
Glia	w^{1118}; *UAS-nls-GFP / + ; repo-Gal4 / +*
CNS	w^{1118}, *elav-Gal4 / + ; UAS-nls-GFP / +*
MNs	w^{1118}; *UAS-nls-GFP / + ; Vglut-Gal4 / +*
PNS	w^{1118}, *elav-Gal4 / + ; UAS-nls-GFP / +*
PNS-da	w^{1118}; *21-7-Gal4* / *UAS-nls-GFP*
Supplemental Figure S2b	
$\alpha Tub84B^{K40A}$	w^{1118}; +; $\alpha Tub84B^{K40A}$ / $\alpha Tub84B^{KO}$
Supplemental Figure S3	
UAS-kat-60	w^{1118}; *ppk-mCD4-tdTomato, ppk-Gal4 / UAS-kat60*
UAS-kat-60 + $dTat^{KO}$	w^{1118}; *ppk-mCD4-tdTomato, ppk-Gal4 / UAS-kat60*; $dTat^{KO}$ / $dTat^{KO}$
Supplemental Figure S4	
$nompC^{1/3}$	w^{1118}; $nompC^{1}$ / $nompC^{3}$
c3da>TnT	w^{1118}; *nompC-Gal4 / UAS-Tetanus Toxin*

Table S4. Related to all figures. Oligonucleotide primers used in this study.	
Primers used to generate dsRNAs.	
T7-GCN5-f	TAATACGACTCACTATAGGTGAGAATTTGGATGACCTGCCTGCGGATGTAGTAATGCGCG
T7-GCN5-r	TAATACGACTCACTATAGGCAGCTATGAACTGCGTGTTCACAATGCTTGGATGCAGC
T7-NAT10-f	TAATACGACTCACTATAGGTCATGGCAAAAAGCGAGCAAAGAAGATTGCTGTGGGC
T7-NAT10-r	TAATACGACTCACTATAGGATTCACTGGCTCCACGTTGATGGTCTTGGAGCTAAGTGGC
T7-ELP3-f	TAATACGACTCACTATAGGTTCCGGCGTGGAACACGGAAATCTCCGTGAACTGGCGC
T7-ELP3-r	TAATACGACTCACTATAGGCTATATATTAATGTATATATTTAAGAGAGTAGTTTTAAG
T7-ARD1-f	TAATACGACTCACTATAGGATGAACATCCGCTGCGCAAAACCGGAAGACCTAATGACC
T7-ARD1-r	TAATACGACTCACTATAGGTCAGCAACAATGGCCATCGTGACCGCTGTGGTTGTGCG
T7-Nat1-f	TAATACGACTCACTATAGGATGCCTTCTAGCGATCCCCTGCCGCCCAAGGAGGGCGCGC
T7-Nat1-r	TAATACGACTCACTATAGGGGCCCTGGTATTTGGTCAGGTGGTCCACGGCCTGCTGC
T7-CG3967/dTAT-f	TAATACGACTCACTATAGGATGGTGGAATTCCGCTTCGATATTAAGCCGCTGTTCGCGC
T7-CG3967/dTAT-r	TAATACGACTCACTATAGGGCACGAAATTGTTCGCTTGCGGAATGATTCGCTTTAATCC
T7-CG17003-f	TAATACGACTCACTATAGGATGGTGGAGTTCGCCTTTGACATTAAGCACCTCTTTCCGC
T7-CG17003-r	TAATACGACTCACTATAGGCCCTGCGGAATGGTGCGGACCAGGCCATAGTGTTTGGC
T7-CAT-control-f	TAATACGACTCACTATAGGATCCCAATGGCATCGTAAAGAACATTTTGAGGC
T7-CAT-control-r	TAATACGACTCACTATAGGGGGCGAAGAAGTTGTCCATATTGGCCA
T7-Sirt2-fwd	TAATACGACTCACTATAGGATGGATAAGGTTCGACGCTTCTTTGCAAACACTCTACATC
T7-Sirt2-rev	TAATACGACTCACTATAGGCCATGTCGTACTCCTTGCGGCACTTAATGC
T7-HDAC6-f	TAATACGACTCACTATAGGATACAGTGCGTCGATTGCTG
T7-HDAC6-r	TAATACGACTCACTATAGGCTTGGGATTGGACTCGAAAA
Primers used to generate recombinant dTAT	
Bam-dTATalt	CCTATAGGATCCATGGTAGAGTTTCGCTTTGACATAAAACCCCTATTTGCTCAACC
dTATalt-196-Not	GGTATAGCGGCCGCTCACCCATTGCCTCCCCCGTTTCCGGACTCTCCGTCATTGAAAAAC
NheI-dTAT	GGTATAGCTAGCTATAATGGTGGAATTCCGCTTCGATATTAAG
dTAT-196-XhoI	GGTATACTCGAGATTCCCCGATTCCCCATCGTTAAAGAATCCCTCGTAGAGCACGAAATT

Primers used to generate UAS-GFP-dTat constructs	
KpnI-eGFP	CCTATAGGTACCATGGTGAGCAAGGGCGAGGAGCTGTTCACCGGGG TGGTGCCC
EcoRI-eGFP	CCTATAGGTACCATGGTGAGCAAGGGCGAGGAGCTGTTCACCGGGG TGGTGCCC
GFP-dTATalt-s	CCTATAGGTACCATGGTGAGCAAGGGCGAGGAGCTGTTCACCGGGG TGGTGCCC
GFP-dTATalt-as	CCTATAGGTACCATGGTGAGCAAGGGCGAGGAGCTGTTCACCGGGG TGGTGCCC
dTATalt-L-Apa	CCTATAGGTACCATGGTGAGCAAGGGCGAGGAGCTGTTCACCGGGG TGGTGCCC
dTATalt-S-ApaI	CCTATAGGTACCATGGTGAGCAAGGGCGAGGAGCTGTTCACCGGGG TGGTGCCC
dTATalt-L-NotI	CCTATAGGTACCATGGTGAGCAAGGGCGAGGAGCTGTTCACCGGGG TGGTGCCC
dTATalt-S-NotI	CCTATAGGTACCATGGTGAGCAAGGGCGAGGAGCTGTTCACCGGGG TGGTGCCC
dTatalt-G133W-G135-W-sense	CCTATAGGTACCATGGTGAGCAAGGGCGAGGAGCTGTTCACCGGGG TGGTGCCC
dTatalt-G133W-G135-W-asense	CCTATAGGTACCATGGTGAGCAAGGGCGAGGAGCTGTTCACCGGGG TGGTGCCC
Primers used for dTat-KO gRNA expression constructs.	
gRNA1F	CTTCAAGAACAATCGGGGTGCAGC
gRNA1R	AAACGCTGCACCCCGATTGTTCTT
gRNA2F	CTTCGAGCAGCGGATTGGGAGCAC
gRNA2R	AAACGTGCTCCCAATCCGCTGCTC
Primers used for constructing the dTat-KO repair template.	
dTatGFP gRNA1 S	CTTCGGGGTCCAAAAGAACAATCG
dTatGFP gRNA1 AS	AAACCGATTGTTCTTTTGGACCCC
dTatGFP gRNA2 S	CTTCGCAAGAGGTATATTTCCTACT
dTatGFP gRNA2 AS	AAACAGTAGGAAATATACCTCTTGC
Primers used for GFP-dTat gRNA expression constructs.	
dTatGFP gRNA1 S	CTTCGGGGTCCAAAAGAACAATCG
dTatGFP gRNA1 AS	AAACCGATTGTTCTTTTGGACCCC
dTatGFP gRNA2 S	CTTCGCAAGAGGTATATTTCCTACT
dTatGFP gRNA2 AS	AAACAGTAGGAAATATACCTCTTGC
Primers used for constructing the GFP-dTat repair template	
dTatGFP 5'arm F	CCCTTCGCTGAAGCAGGTGGGGTTGTGCGACTACCACTC
dTatGFP 5'arm R	CTCCTTTACTCATTATGCTGCATCCCGATTG
dTatGFP GFP F	GGGATGCAGCATAATGAGTAAAGGAGAAGAACTTTTC
dTatGFP GFP R	GGAATTCCACCATTTTGTATAGTTCATCCATGC
dTatGFP start F	TGAACTATACAAAATGGTGGAATTCCGCTTC
dTatGFP start R	ATGTCCGCGGCCGCTAGCATGCAAGCATTACTTACTTGTGACCCGC
dTatGFP 3'arm F	TAGGCCTTCTGCAGCGCAAGTAGGAAATATACCTC
dTatGFP 3'arm R	GATTGACGGAAGAGCCTCATTGGTTAACAGTTAGC